

Spectroscopic studies of globular clusters in dwarf galaxies

Sharina M.E.¹, Shimansky V.V.²

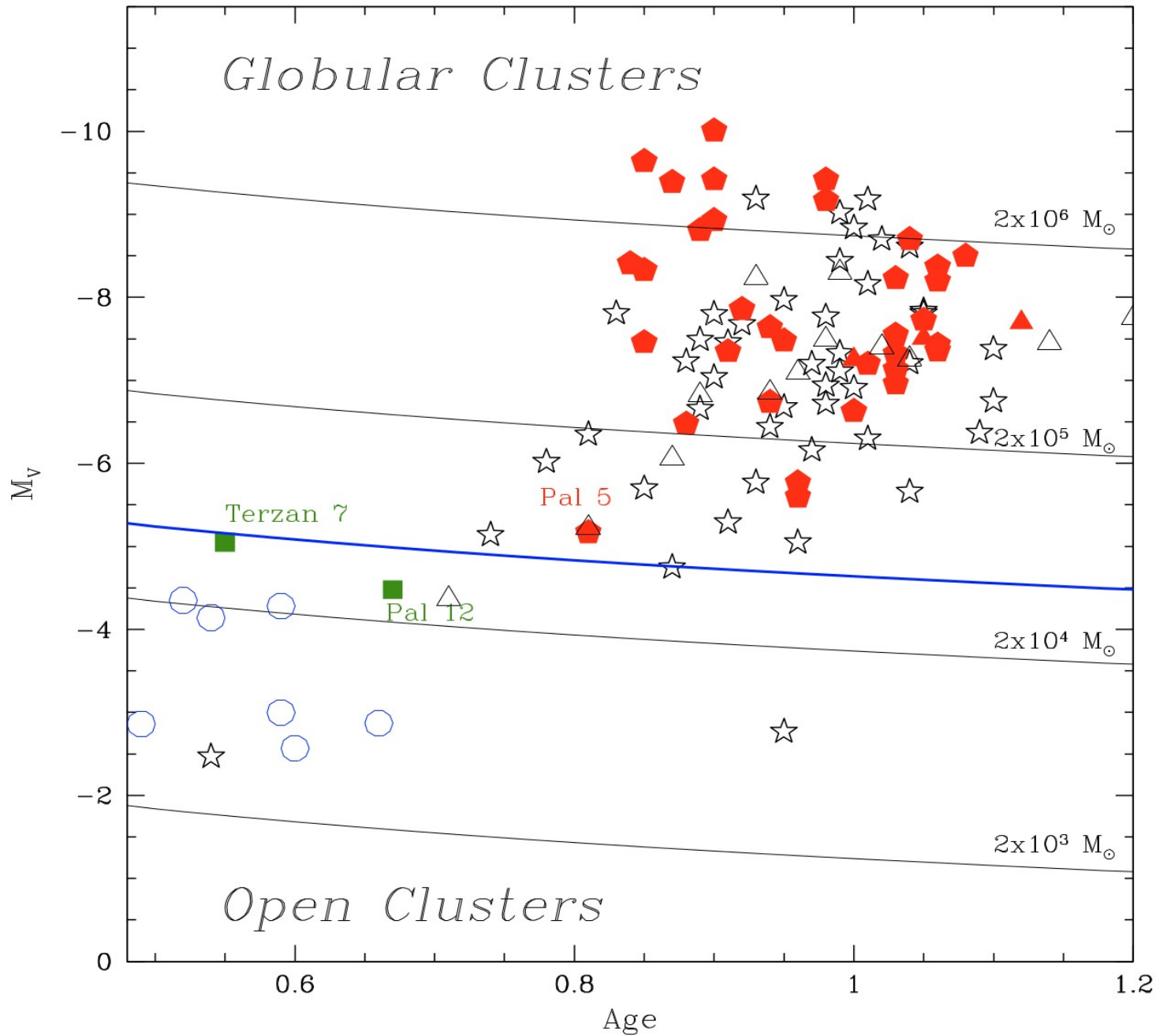
¹Special Astrophysical Observatory RAS, Nizhnij Arkhyz, 369167 Russia

²Kazan (Volga Region) Federal University, Kazan, 420008 Russia

sme@sao.ru, Slava.Shimansky@kpfu.ru

An overview of recent studies of globular clusters (GCs) in dwarf galaxies shows the significance of these objects for understanding the evolution of the host galaxies. In particular, we present the results of 6-m telescope (BTA) medium-resolution observations of four GCs in the dwarf spheroidal galaxy IKN. We have derived radial velocities, ages, metallicities and Mg, Ca and C elemental abundances. We judge about the horizontal branch types of the studied extragalactic GCs using the information gained from the spectra.

Globular and open clusters



GCs with multiple stellar populations are shown in red

Hubble Space Telescope Imaging of Globular Cluster Candidates in Low Surface Brightness Dwarf Galaxies

Sharina M.E., Puzia T.H.,
Makarov D.I.

Abstract. Fifty-seven nearby low surface brightness dwarf galaxies ($-10 > M_V > -16$) were searched for globular cluster candidates using Hubble Space Telescope WFPC2 imaging in V and I. The sample consists of 18 dwarf spheroidal (dSph), 36 irregular (dIrr), and 3 "transition" type (dIrr/dSph) galaxies with angular sizes less than 3.7 kpc situated at distances 2-6 Mpc in the field and in the nearby groups: M81, Centaurus A, Sculptor, Canes Venatici cloud...

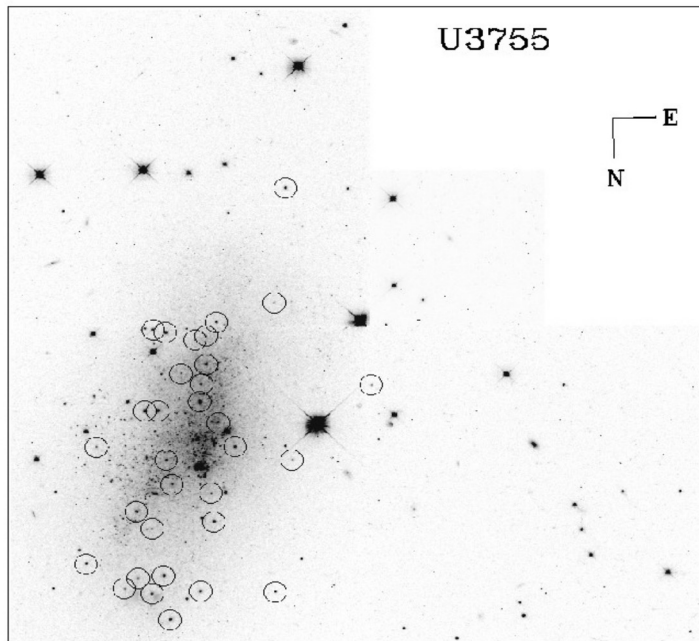


Fig.1a

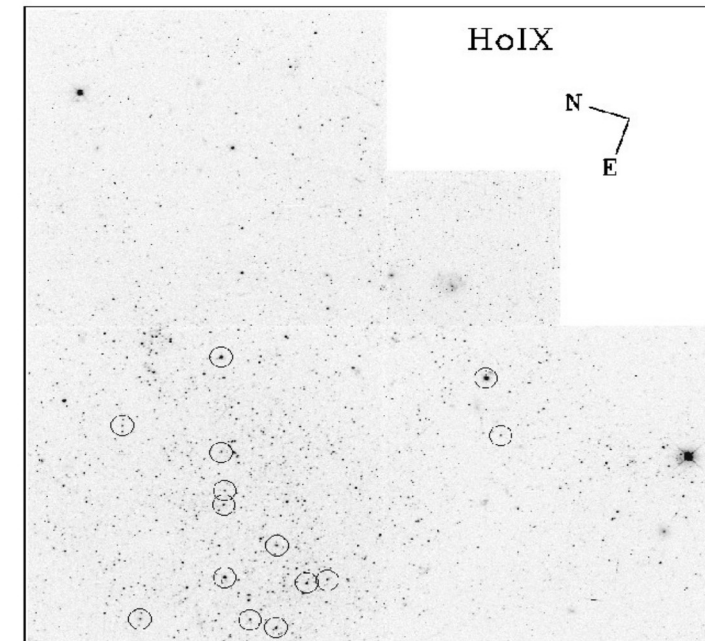
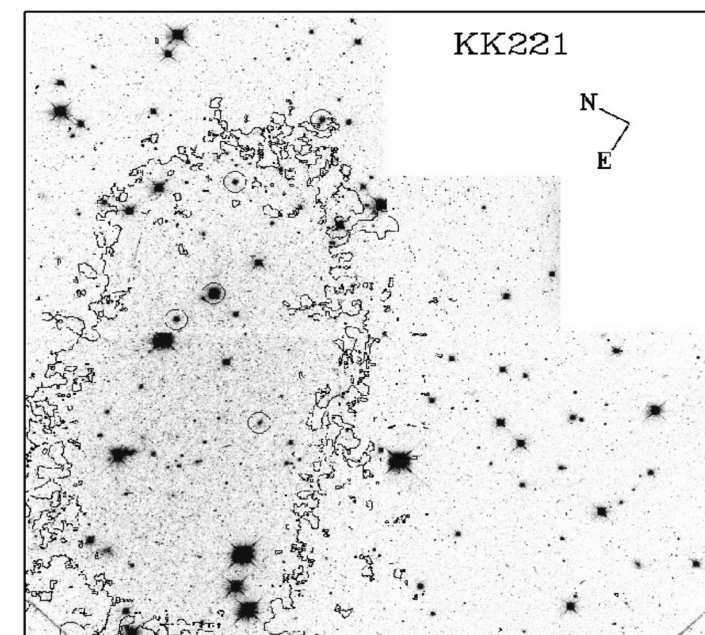
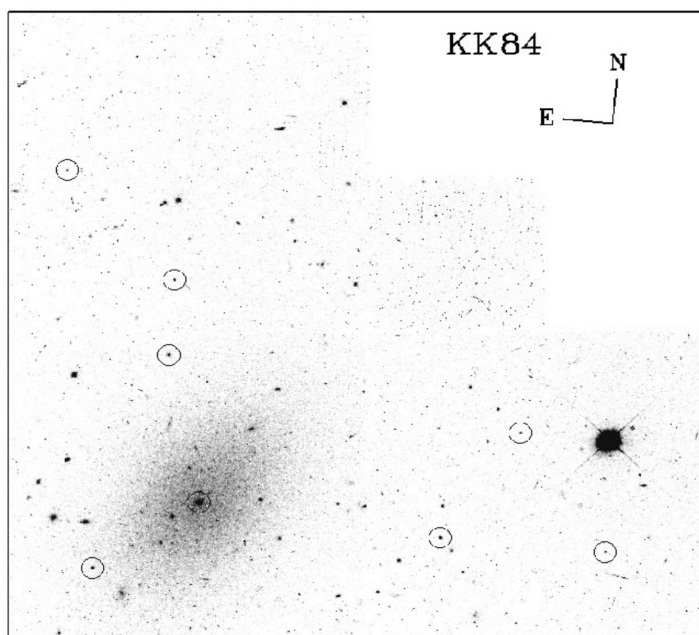


Fig.1b



Globular cluster systems in nearby dwarf galaxies – II. Nuclear star clusters and their relation to massive Galactic globular clusters

I. Y. Georgiev et al.

175 GC candidates in 36 dwarf galaxies

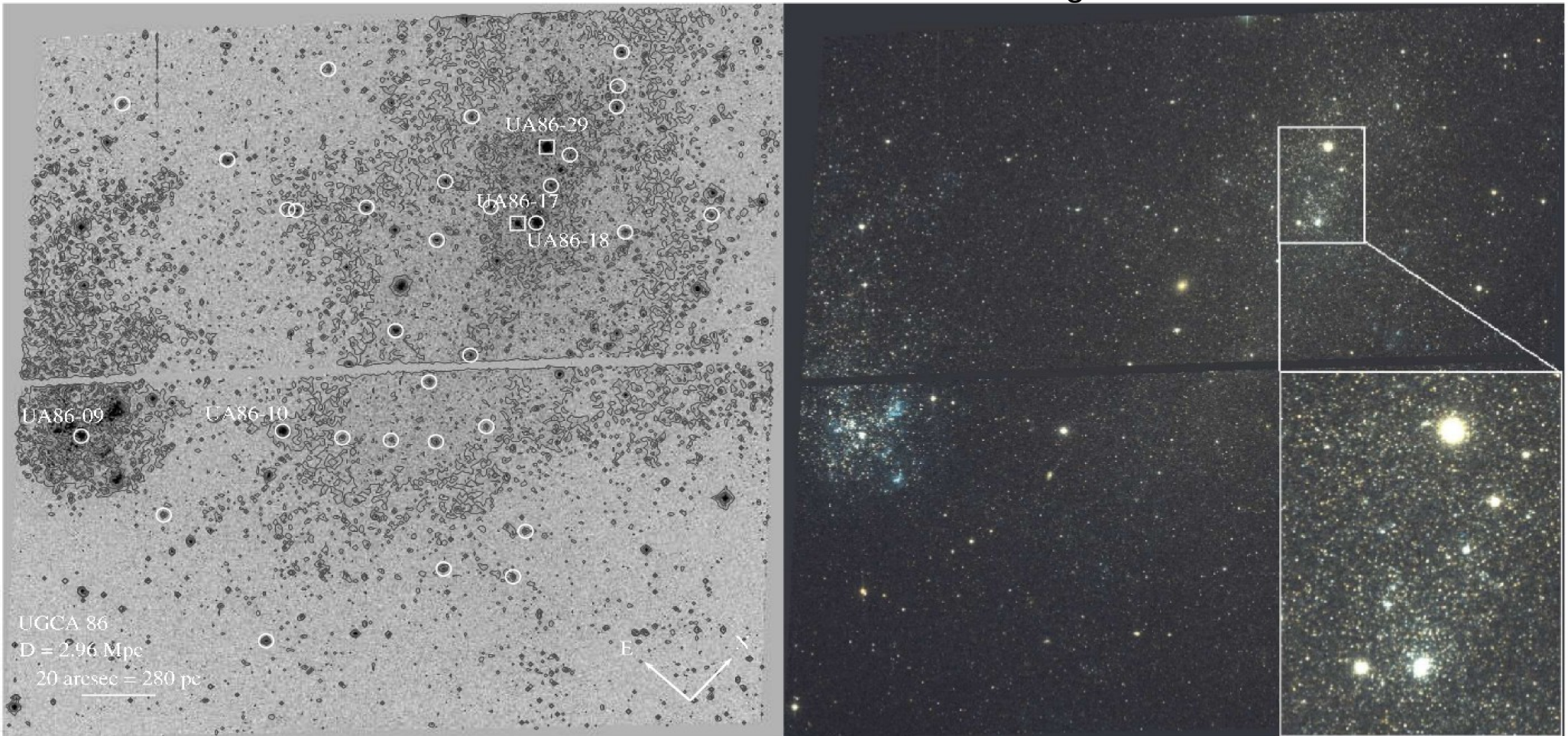
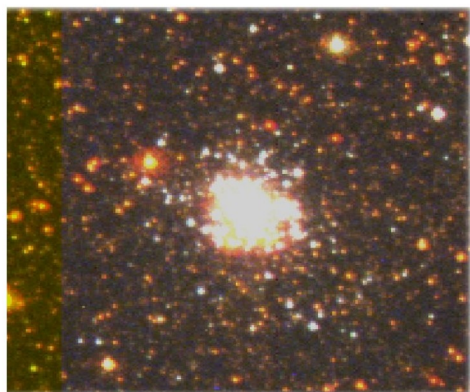
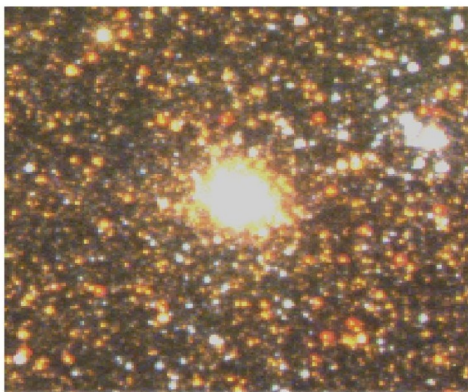


Figure 2. *Left:* Gray scale F606W band HST/ACS image of UGCA 86. White circles mark all GC candidates selected in Georgiev et al. (2009) while the white squares show the two clusters in the nuclear region of UGCA 86. Labeled are all clusters brighter than $M_V = -9$ mag. At least three more star clusters are as luminous as the nGCs, but have colours of $V - I < 0.6$ mag corresponding to an age of < 2 Gyr at $[Fe/H] > -2.3$ dex. The lowest iso-intensity contour corresponds to 10σ above the background. *Right:* colour composite image from F606W, F814W and their average in the blue, red and green channels,

Diversity of star cluster morphologies in IC10 (Sharina et al. 2010, 2010MNRAS.405..839S)



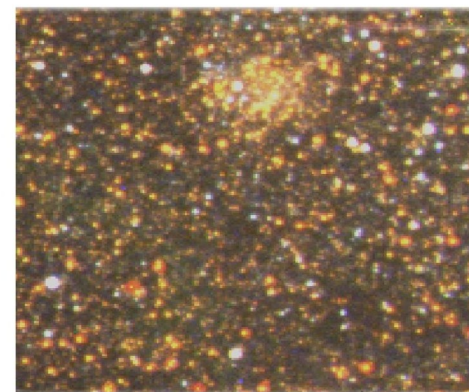
00 20 12.45,+59 17 28.0, **20**



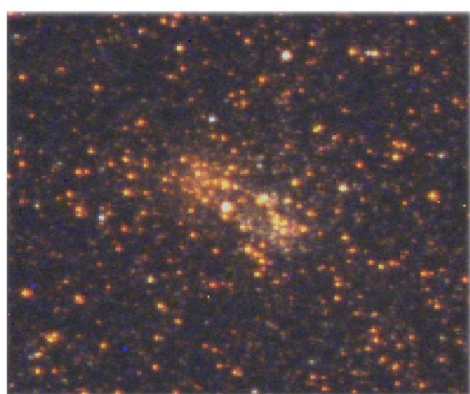
00 20 17.24,+59 17 45.3, **25**



00 20 17.91,+59 19 49.5, **27**



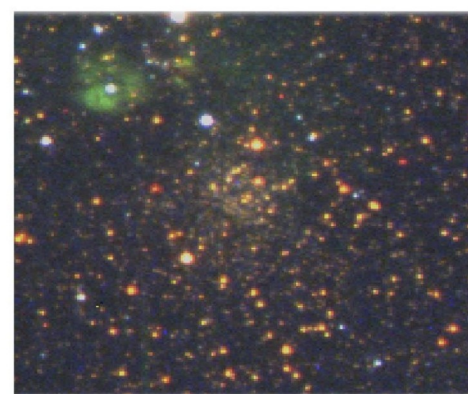
00 20 19.33,+59 17 30.6, **29**



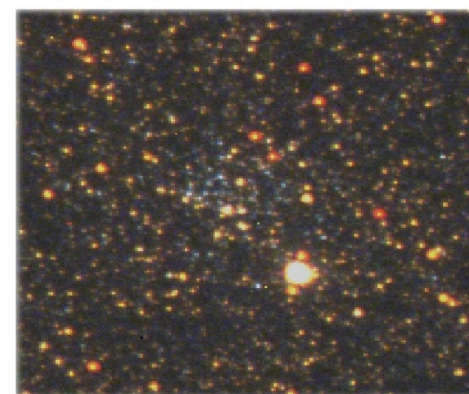
00 20 05.76,+59 18 26.0, **12**



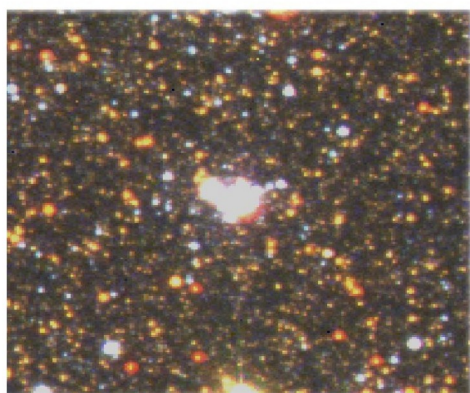
00 20 32.50,+59 17 12.8, **d23**



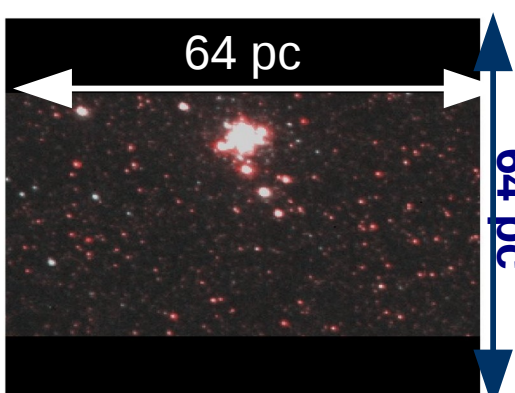
00 20 13.44,+59 20 16.1, **21**



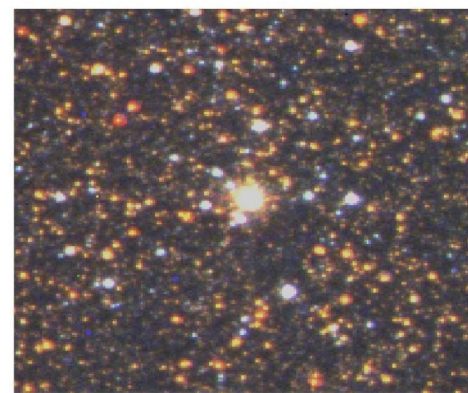
00 20 24.36,+59 19 10.1, **H2-2**



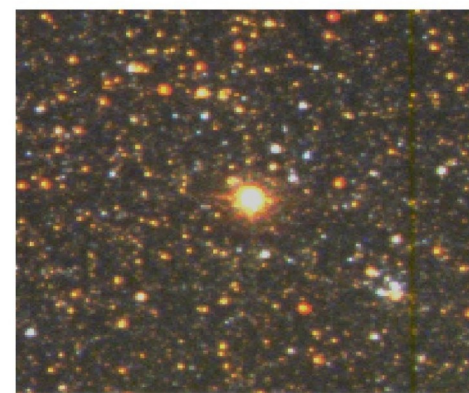
00 20 24.62,+59 18 11.9, **H1-2**



00 20 09.72 +59 17 19.3, **18**



00 20 21.53,+59 18 33.1, **33**



00 20 26.51,+59 16 36.3, **H4-6**

See also Tikhonov, N. A.; Galazutdinova, O. A. 2009AstL...35..748T

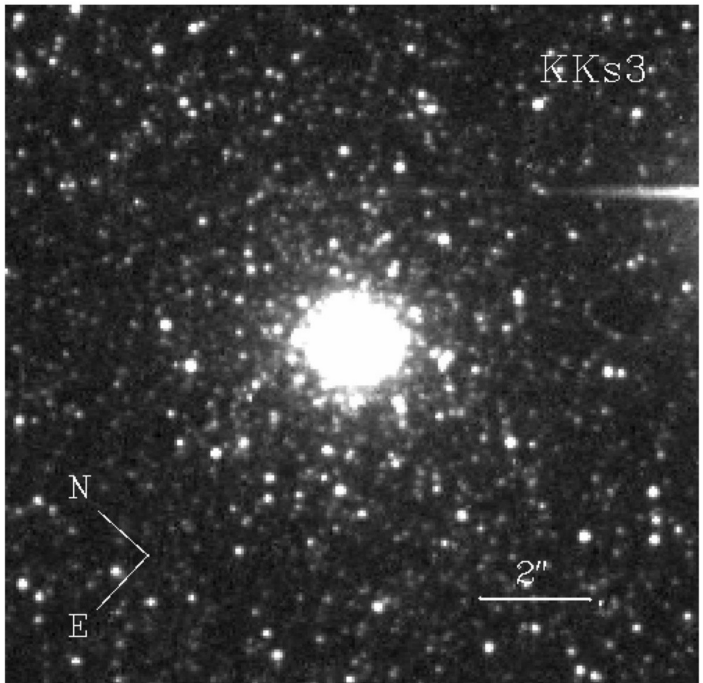
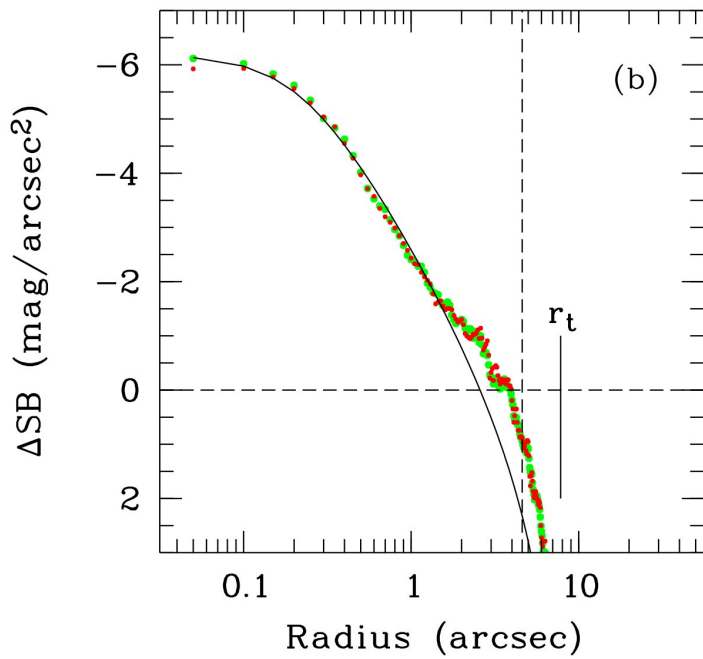
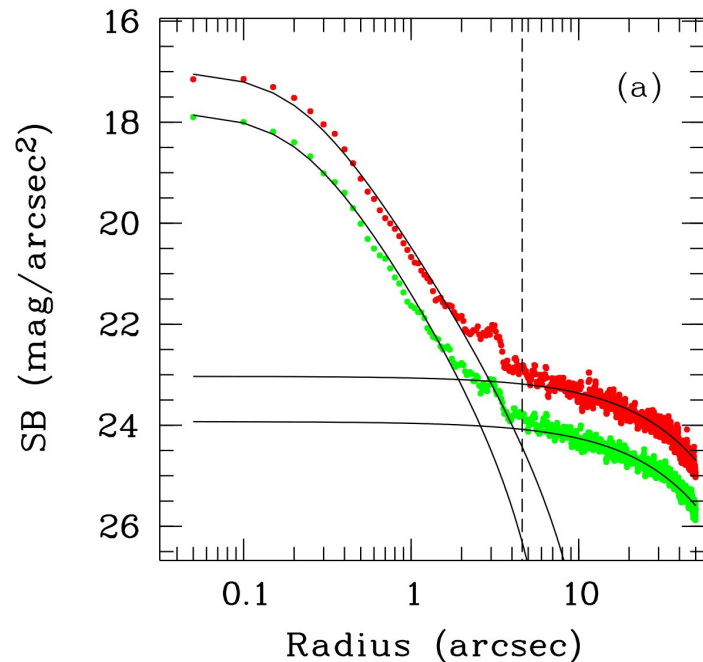


Figure 6. F606W ACS image of the central GC in KKs 3.

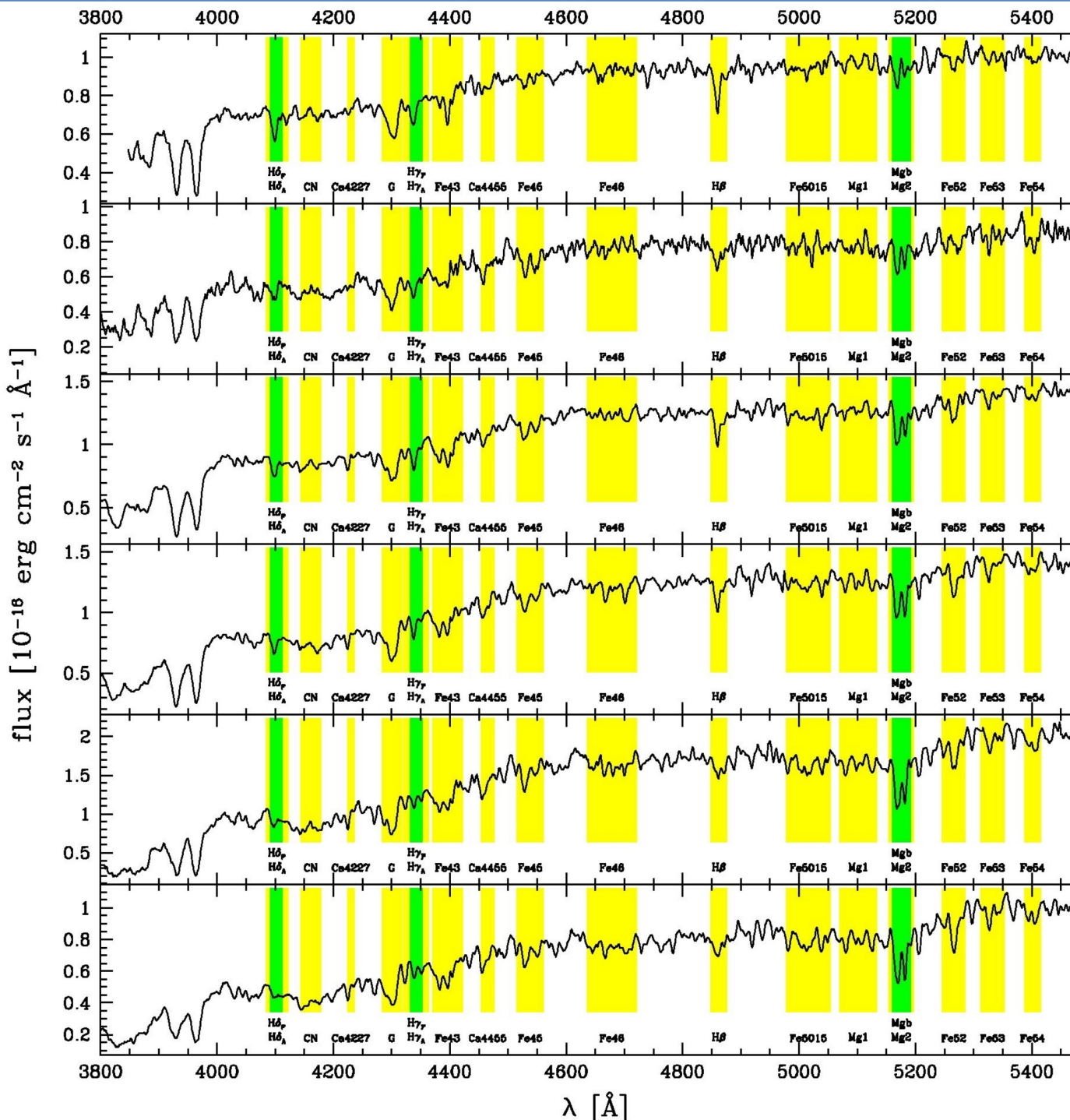
Figure 7. (a) Azimuthally averaged surface brightness profiles of the central region of KKs 3 in the V and I bands (dots). Solid lines show a decomposition of the profile inside the fit range represented by the exponential function and the King (1962) law. (b) The same as in (a), but after subtraction of the galactic contribution. The horizontal dashed line is a zero line. The vertical dashed line in panels (a) and (b) marks the radius ($R \sim 4.6$ arcsec) at which the galactic contribution begins to prevail.

Table 9. Structural parameters of GC in KKs 3 measured using the King (1962) law: central surface brightness in mag arcsec^{-2} , core, and tidal radii in arcsec.

μ_V^0	μ_I^0	r_c	r_t
17.74 ± 0.02	16.97 ± 0.02	0.22 ± 0.01	7.8 ± 4.7



Lick-IDS System (Worley 1994, Worley & Ottaviani 1997)



Lick indices are analogs of equivalent widths:

$$I(\lambda) = \left(1 - \frac{\int F_l(\lambda) \Delta\lambda}{\int F_c(\lambda) \Delta\lambda} \right) \Delta\lambda,$$

where λ is the wavelength, F_l is the flux in the line, and F_c the flux in the continuum in the vicinity of the line
(Burstein et al. 1984; Worley et al. 1994; Worley 1994; Worley & Ottaviani 1997; Trager et al. 1998)

The influence of metallicity on the relative intensity of the Balmer lines and lines of metals
(Puzia et al. 2004)

Lick index system

<http://astro.wsu.edu/worthey/html/index.table.html>

##	Index band	blue continuum	red continuum	name
01	4142.125 - 4177.125	4080.125 - 4117.625	4244.125 - 4284.125	CN_1
02	4142.125 - 4177.125	4083.875 - 4096.375	4244.125 - 4284.125	CN_2
03	4222.250 - 4234.750	4211.000 - 4219.750	4241.000 - 4251.000	Ca4227
04	4281.375 - 4316.375	4266.375 - 4282.625	4318.875 - 4335.125	G4300
05	4369.125 - 4420.375	4359.125 - 4370.375	4442.875 - 4455.375	Fe4383
06	4452.125 - 4474.625	4445.875 - 4454.625	4477.125 - 4492.125	Ca4455
07	4514.250 - 4559.250	4504.250 - 4514.250	4560.500 - 4579.250	Fe4531
08	4634.000 - 4720.250	4611.500 - 4630.250	4742.750 - 4756.500	Fe4668
09	4847.875 - 4876.625	4827.875 - 4847.875	4876.625 - 4891.625	H_beta
10	4977.750 - 5054.000	4946.500 - 4977.750	5054.000 - 5065.250	Fe5015
11	5069.125 - 5134.125	4895.125 - 4957.625	5301.125 - 5366.125	Mg_1
12	5154.125 - 5196.625	4895.125 - 4957.625	5301.125 - 5366.125	Mg_2
13	5160.125 - 5192.625	5142.625 - 5161.375	5191.375 - 5206.375	Mg_b
14	5245.650 - 5285.650	5233.150 - 5248.150	5285.650 - 5318.150	Fe5270
15	5312.125 - 5352.125	5304.625 - 5315.875	5353.375 - 5363.375	Fe5335
16	5387.500 - 5415.000	5376.250 - 5387.500	5415.000 - 5425.000	Fe5406
17	5696.625 - 5720.375	5672.875 - 5696.625	5722.875 - 5736.625	Fe5709
18	5776.625 - 5796.625	5765.375 - 5775.375	5797.875 - 5811.625	Fe5782
19	5876.875 - 5909.375	5860.625 - 5875.625	5922.125 - 5948.125	Na_D
20	5936.625 - 5994.125	5816.625 - 5849.125	6038.625 - 6103.625	TiO_1
21	6189.625 - 6272.125	6066.625 - 6141.625	6372.625 - 6415.125	TiO_2
22	4083.500 - 4122.250	4041.600 - 4079.750	4128.500 - 4161.000	Hdelta_A
23	4319.750 - 4363.500	4283.500 - 4319.750	4367.250 - 4419.750	Hgamma_A
24	4091.000 - 4112.250	4057.250 - 4088.500	4114.750 - 4137.250	Hdelta_F
25	4331.250 - 4352.250	4283.500 - 4319.750	4354.750 - 4384.750	Hgamma_F

VLT SPECTROSCOPY OF 27 GLOBULAR CLUSTERS IN 5 LSB DWARF GALAXIES, Puzia T.H., Sharina M.E., ApJ, 674, 909 (2008)

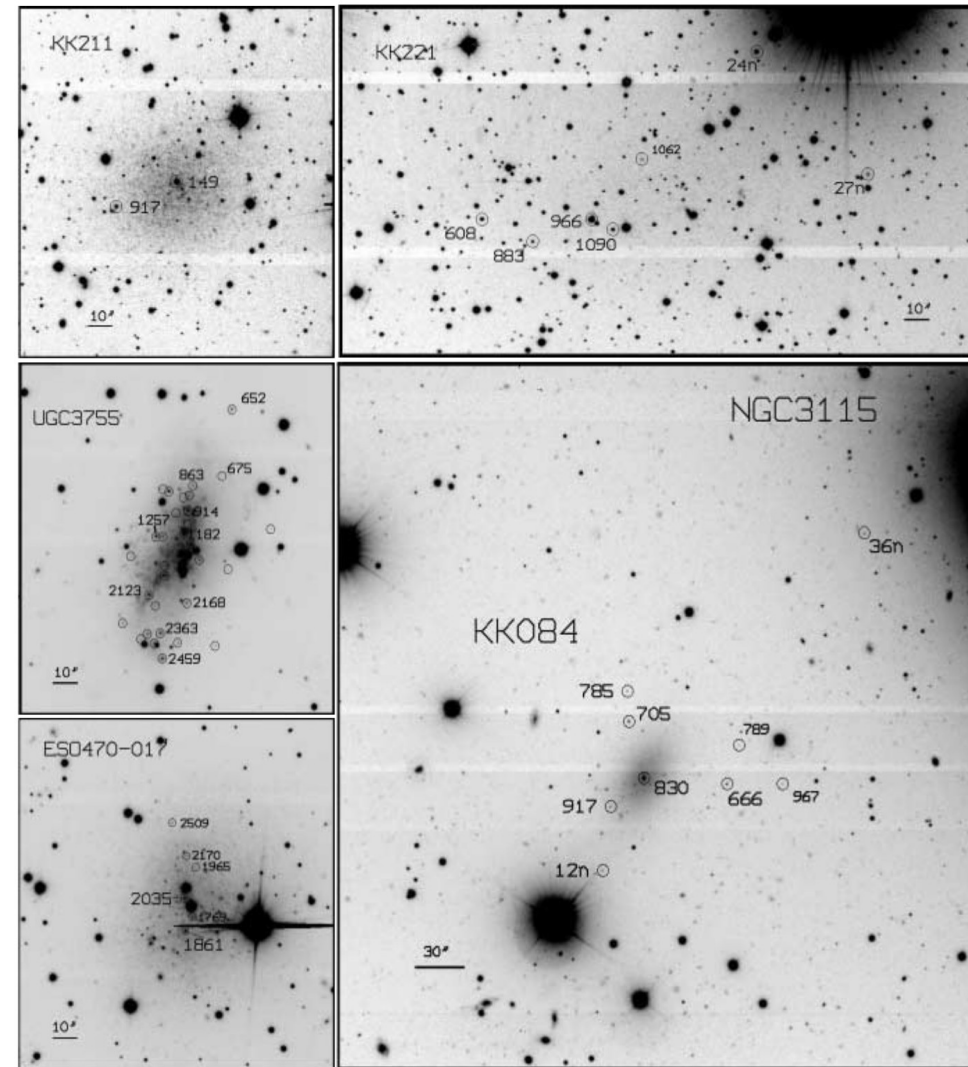
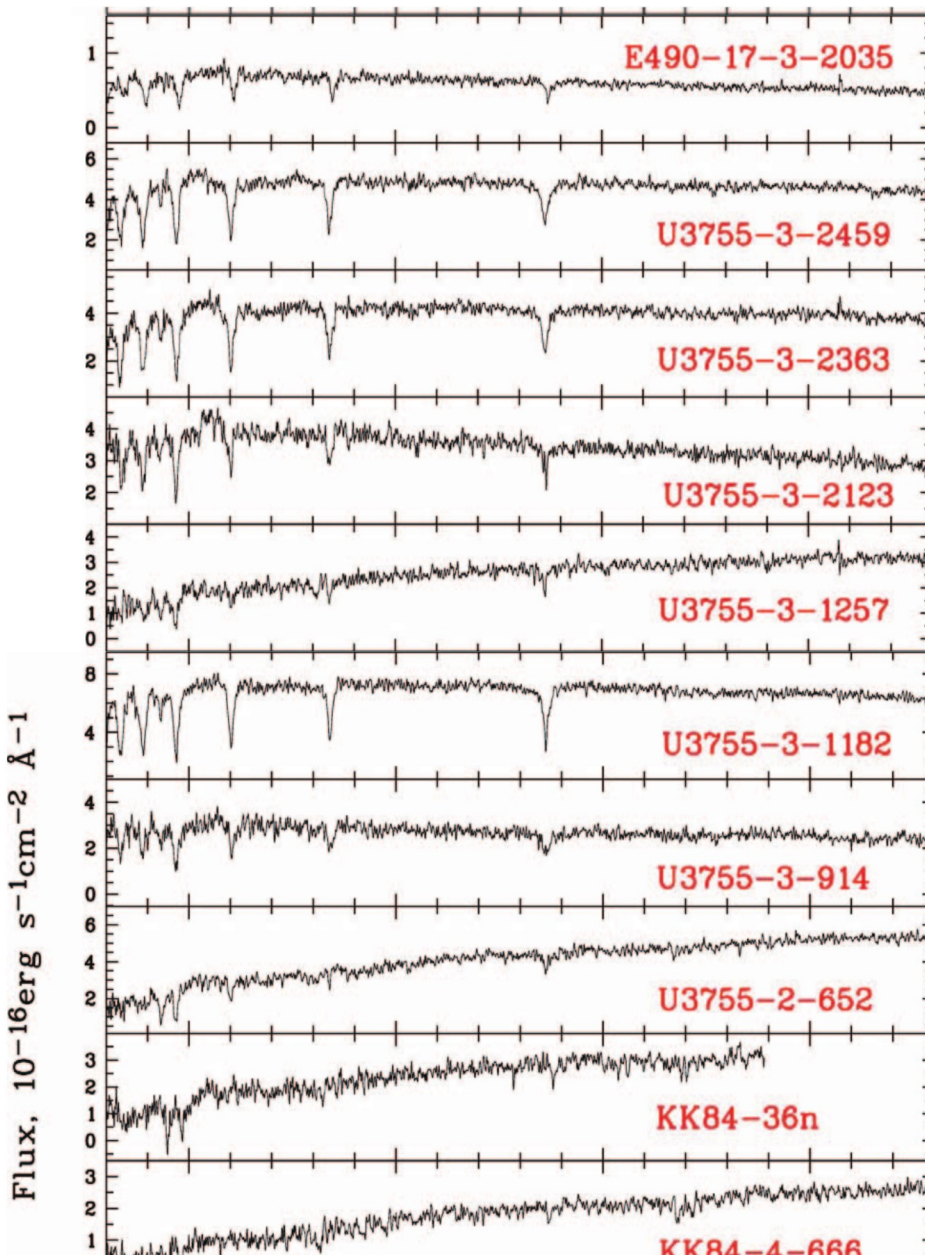
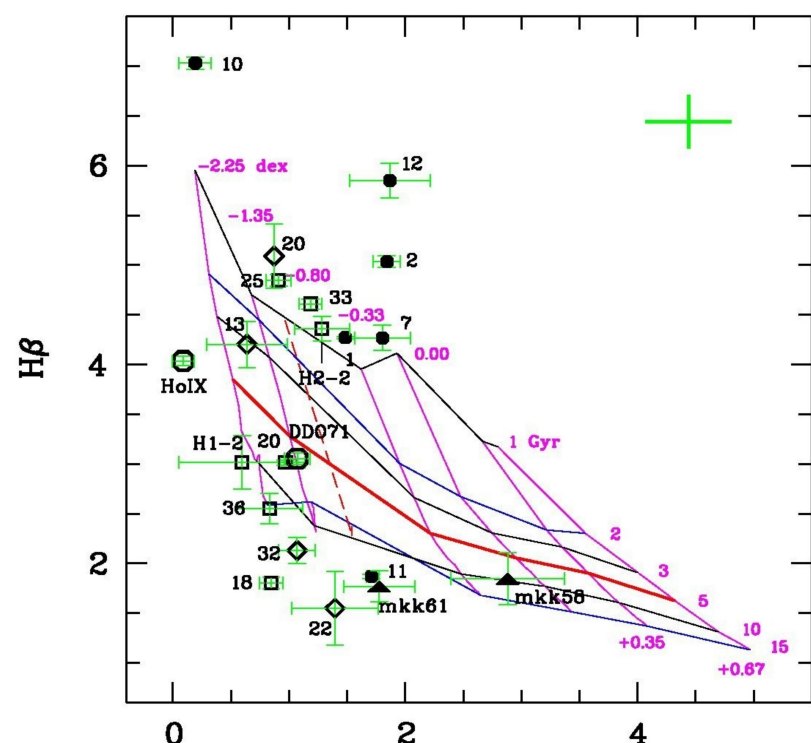


FIG. 2.—FORST-2 images of our sample dwarf galaxies with marked GCs. North is to the top, and east is on the left. The objects are labeled according to Table 5.

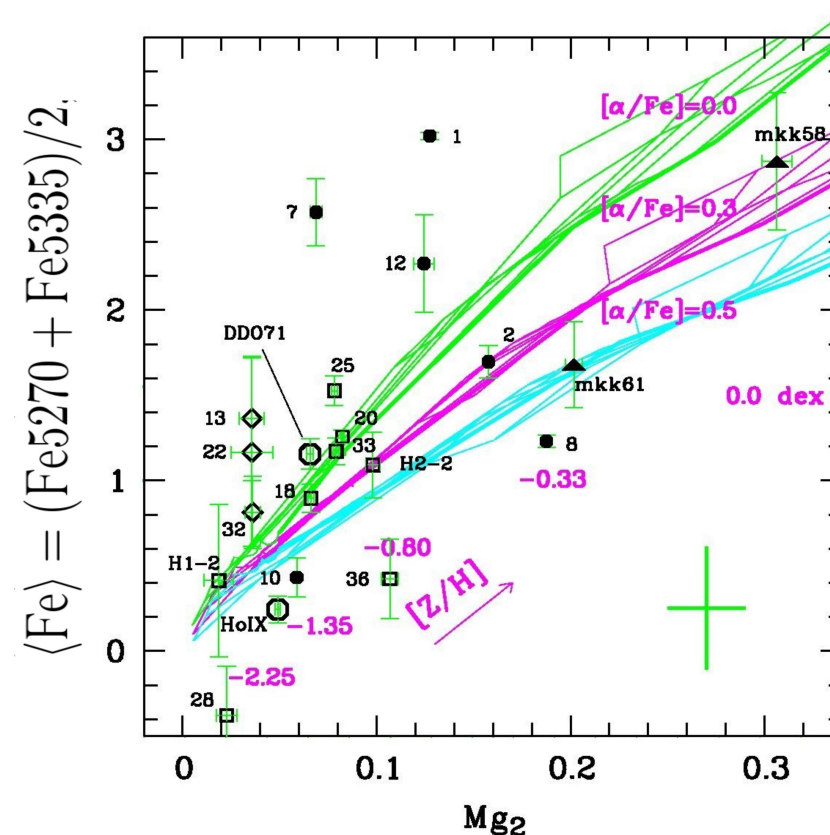
to robustly quantify the excess of clusters with respect to GCs and

SAO RAS 6-m telescope spectroscopic observations of globular clusters in nearby galaxies

We present the results of medium-resolution spectroscopy of 28 globular clusters (GCs) in six nearby galaxies of different luminosities and morphological types, situated in M33 (15 objects), M31 (three), IC10 (four), UGCA86 (four), Holmberg IX (one) and DDO71 (one) obtained at the Special Astrophysical Observatory 6-m telescope...



$$[\text{Mg}/\text{Fe}]' = \sqrt{(\text{Mgb} \cdot (0.72\text{Fe}5270 + 0.28\text{Fe}5335))}$$



SSP models by Thomas et al. (2003, 2004)

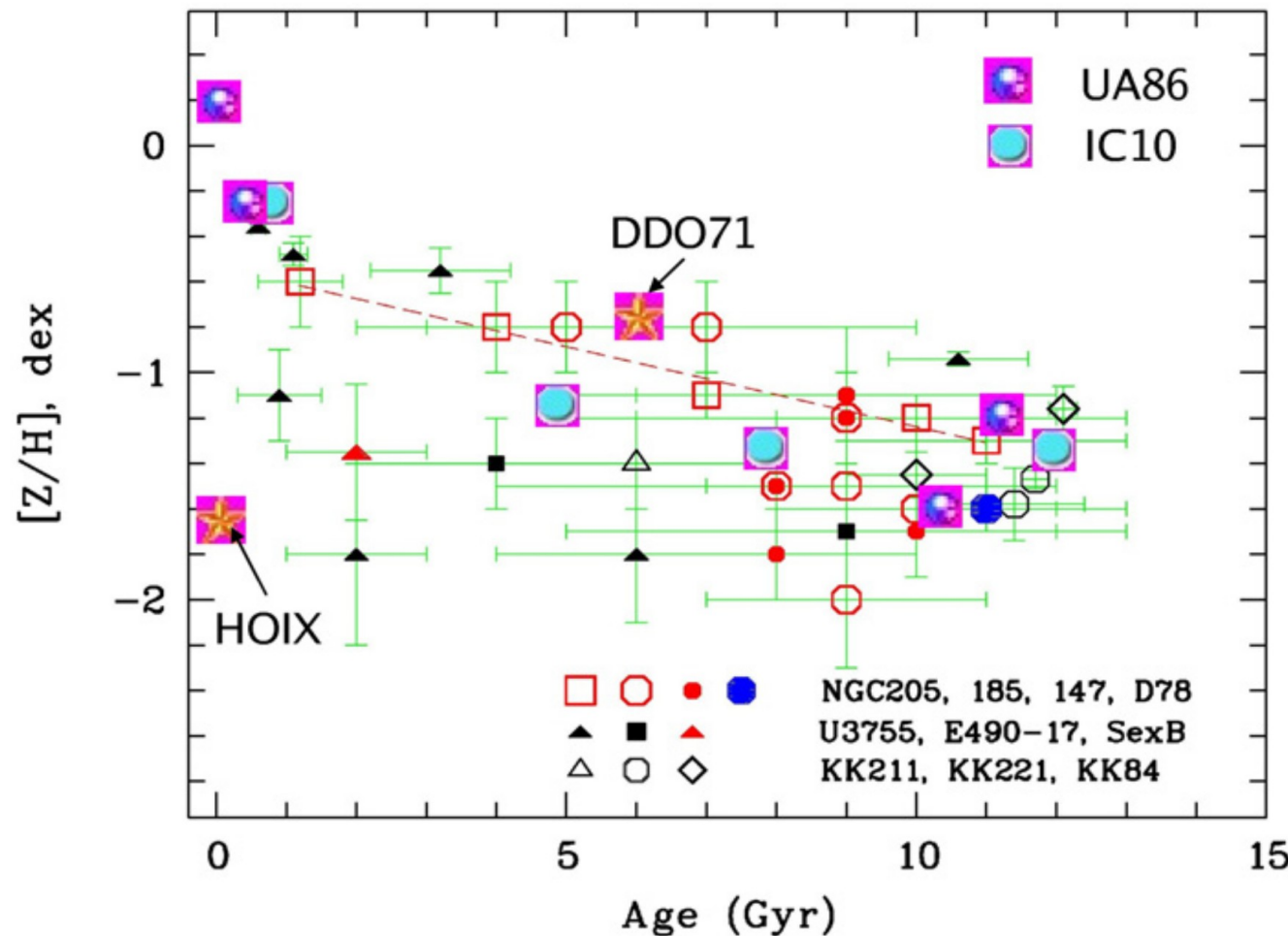


Fig. 1. Age-metallicity relation for globular clusters in LSB dwarf galaxies, and in the satellites of M 31: NGC 147, 185, and 205 (Sharina *et al.* 2003, 2006; Puzia & Sharina 2008). The red line shows the linear regression for GCs in NGC 205. It corresponds well the closed-box model of continuous star formation (see text for details).

Conclusions from the analysis of Lick indices for GCs in dwarf galaxies

- Spreads of ages and spreads of metallicities are larger for GCs in more massive galaxies
- Mean [a/Fe] of GCs are larger in more massive galaxies
- Metal-rich GCs occur in galaxies with Mass>10^9 Msun
- [a/Fe] of oldest GCs in dwarf and normal galaxies are similar
- GCs in dEs are more metal-rich on average, than GCs in dIrrs.

(Sharina et al., 2010vsgh.conf..181S)

Spectroscopy of Globular Clusters in dSph IKN

2019ARep...63..687S

Observational properties of IKN (ultra-diffuse galaxy, Karachensev et al. 2017)

$D,$ Mpc	$M_B,$ mag	$A_e,$ kpc	$SB_{Be},$ mag/ \square''	Diam., kpc	$V_h,$ km/s
3.75	-11.6	3.2	27.2	8.6	38 ± 30

(M-m)₀=27.87 mag

$V_r = -140$ km/s
(Chiboucas et al., 2009)

↑
(This work)

Properties of globular clusters in IKN (Georgiev et al., 2009)

Object	$\alpha(2000)$	$\delta(2000)$	M_V	$V - I$	r_h, pc
IKN5	$10^h 08^m 05.5s^s$	$+68^\circ 24' 58''$	-8.47^m	0.91^m	2.9
IKN4	10 08 04.8	$+68^\circ 24' 54''$	-7.41	0.94	2.0
IKN3	10 08 05.3	$+68^\circ 24' 34''$	-6.76	1.09	14.8
IKN1	10 08 07.1	$+68^\circ 23' 37''$	-6.65	0.91	6.6

Spectroscopy of Globular Clusters in dSph IKN

2019ARep...63..687S

6-m telescope observations 2013 – 2015. Texp (total) ~ 15 hours.

SCORPIO-1 multi-mode primary-focus focal reducer (Afanasiev & Moiseev (2005)

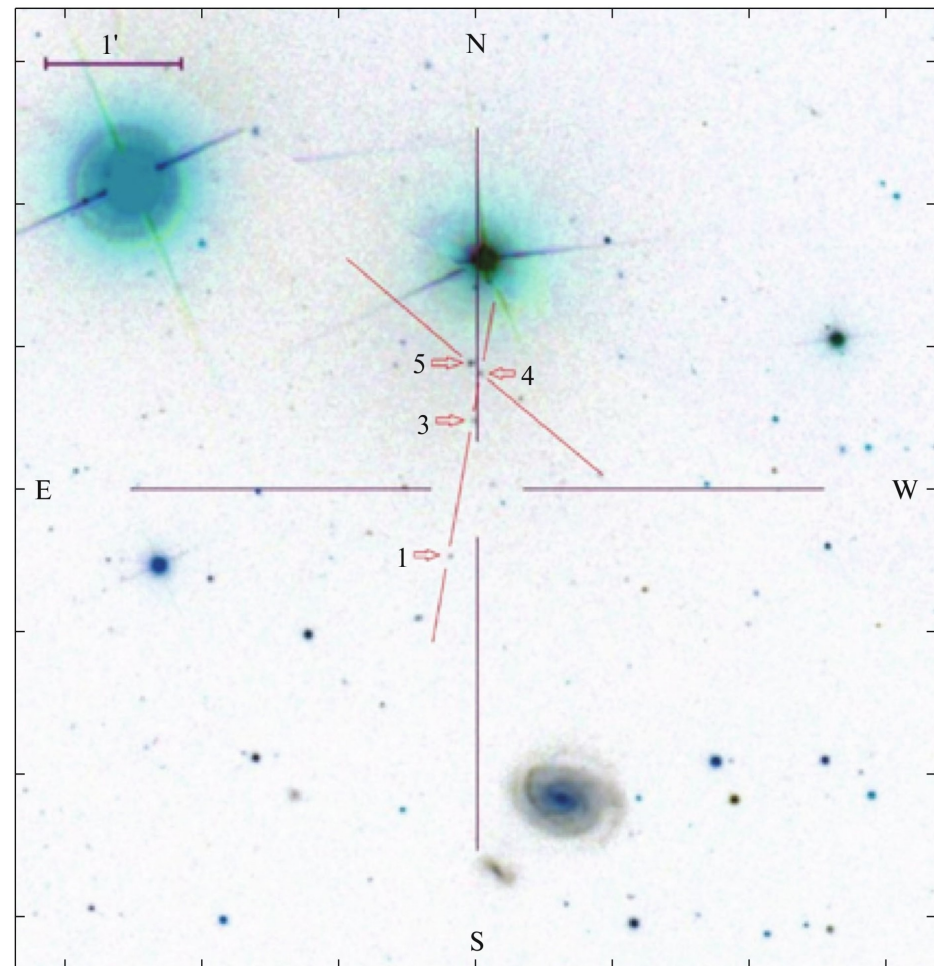
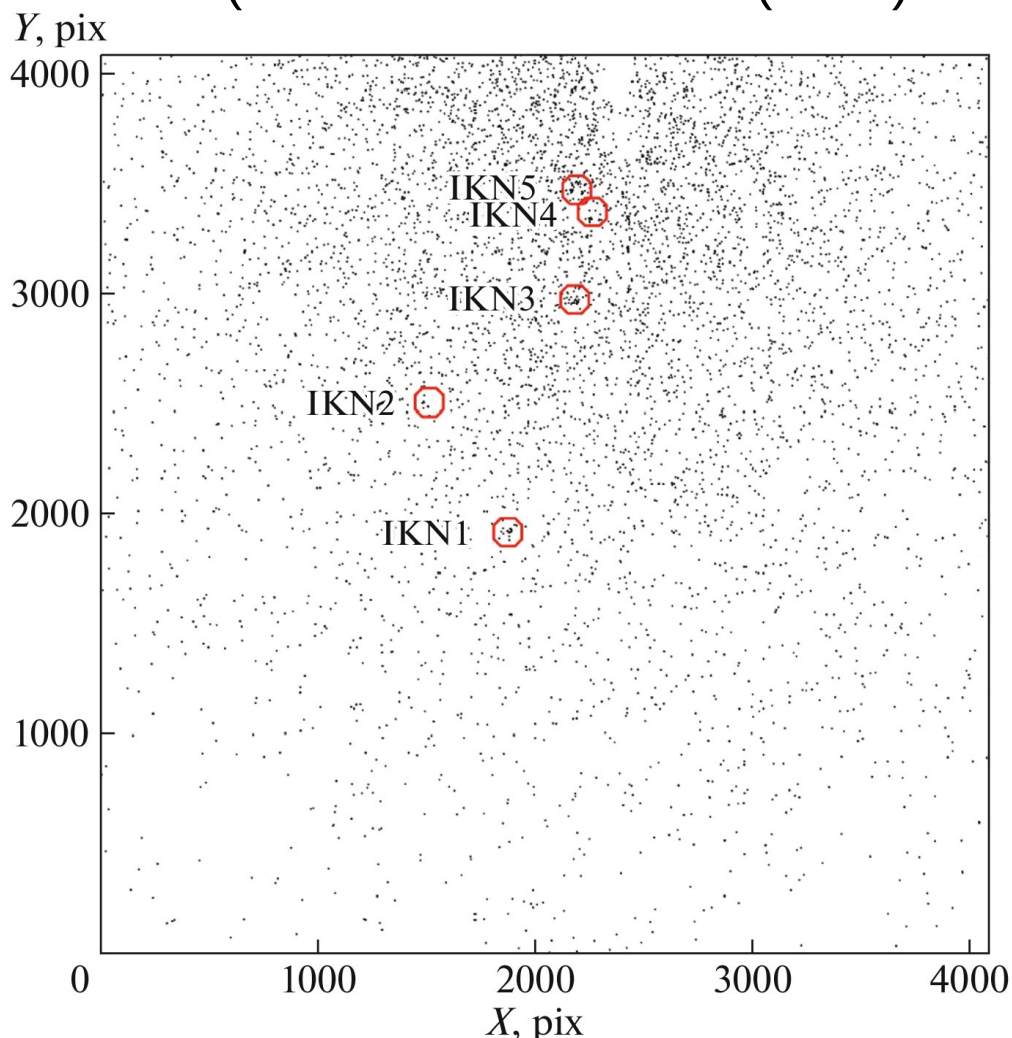


Illustration of the positioning of the slits on the SDSS color image. The globular clusters are indicated.



Distribution of RGB $I < -5.5$ mag.
GCs from Georgiev et al., 2009)

Observational data

Globular clusters in IKN were observed with the 6-m telescope of the Special Astrophysical Observatory (SAO) using the SCORPIO-1 multi-mode, primary-focus focal reducer (Afanasiev & Moiseev, 2005) in spectroscopic mode with a long slit with width 1''. The VPHG1200G grating was used for the 2013 observations, and the VPHG1200B grating for the 2014–2015 observations.

The gratings we used have 1200 lines/mm, and provide a spectral resolution of $\text{FWHM} \sim 5 - 5.5 \text{ \AA}$ and a dispersion of $0.87 - 0.88 \text{ \AA/pixel}$.

The wavelength ranges are $\sim 3900 - 5500 \text{ \AA}$ for VPHG1200B and $\sim 4000 - 5700 \text{ \AA}$ for VPHG1200G.

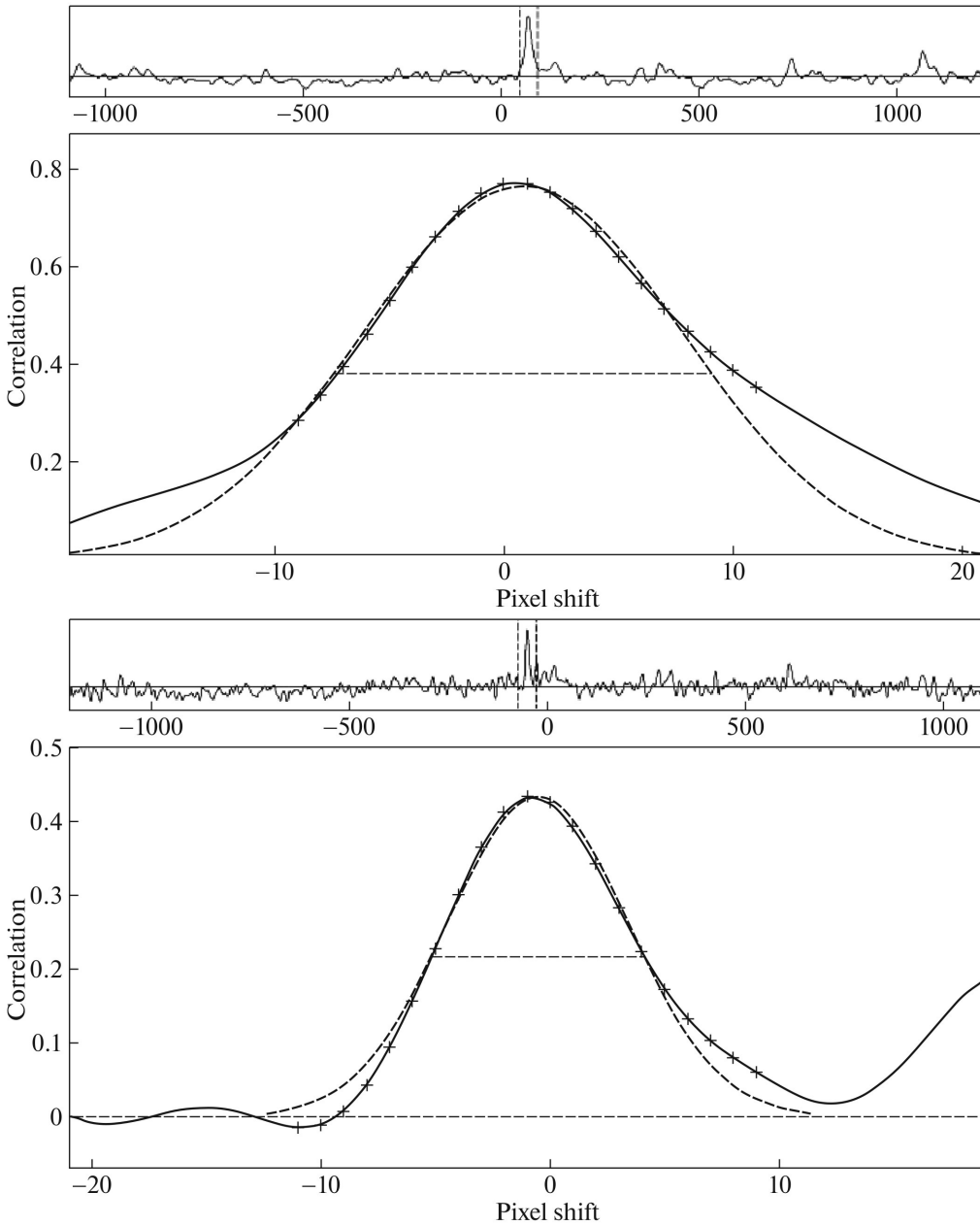
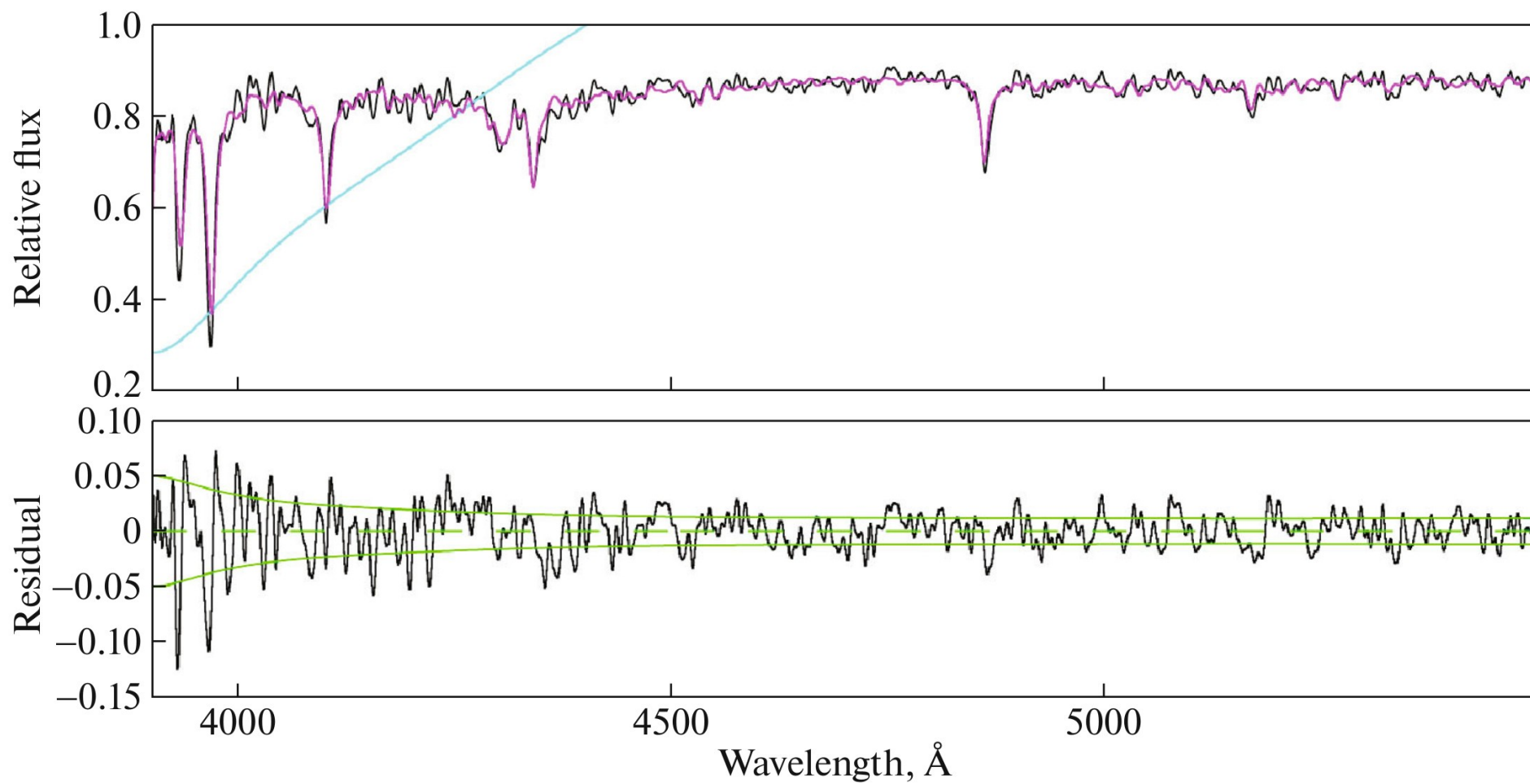


Table 4. Radial velocities of the IKN clusters derived from spectra obtained on different nights

Object	Date	V_r , km/s
IKN4 + IKN5	14.03.2013	27 ± 37
IKN3 + IKN1	15.03.2013	-20 ± 54
IKN4	01.02.2014	72 ± 43
IKN3 + IKN1	01.02.2014	-23 ± 51
IKN5	01.02.2014	44 ± 13
IKN3 + IKN1	15.02.2015	12 ± 49
IKN4	15.02.2015	35 ± 35
IKN3	15.02.2015	14 ± 50
IKN1	15.02.2015	-38 ± 52
IKN5	18.02.2015	14 ± 46
IKN4	18.02.2015	2 ± 50
IKN3	18.02.2015	-21 ± 55
IKN1	18.02.2015	-13 ± 50
IKN1 + IKN3	18.02.2015	-44 ± 36

Fig. 3. Cross-correlation of the integrated spectra of IKN4 + IKN5 (upper) and IKN1 + IKN3 (lower) with spectra of the twilight sky. The top panels of each of the plots show the full cross-correlation functions. The vertical dashed lines mark the boundaries of the sections of the functions shown in the lower panels. The intensities of the cross-correlation peaks are plotted on the vertical axes. The offsets between the spectra of the object and of the radial-velocity standard in pixels (scales at the bottom of the figures) and in km/s (scales at the top of the lower panels) are plotted along the horizontal axes in the lower panels. The dashed lines in the lower panels show the results of Gaussian fitting of the cross-correlation peaks.

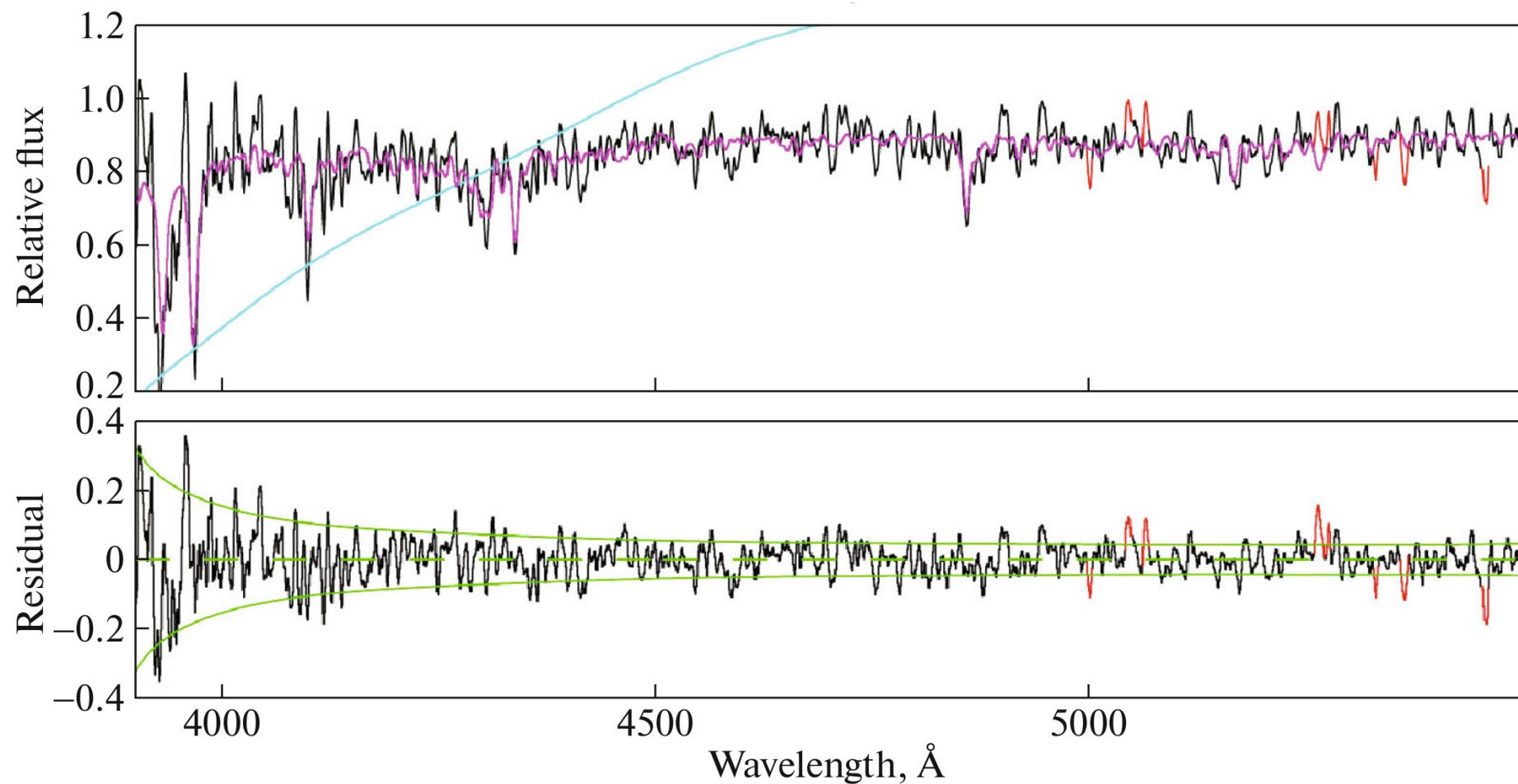
IKN5 + IKN4 vs. NGC 6341 ([Fe/H] = -2.28), HBR= (B-R)/(B+V+R)= 0.9)



Comparison of the integrated spectrum of **IKN5 + IKN4** with the medium-resolution spectrum of NGC6341 (Sharina et al. 2018). The results of dividing the spectra of objects by the corresponding model spectra are partially visible, shown by thin solid lines. The lower panels display the results obtained by subtracting the model spectra from the observed cluster spectra. The solid curves in the lower panels show the envelope corresponding to $S/N \sim 65$.

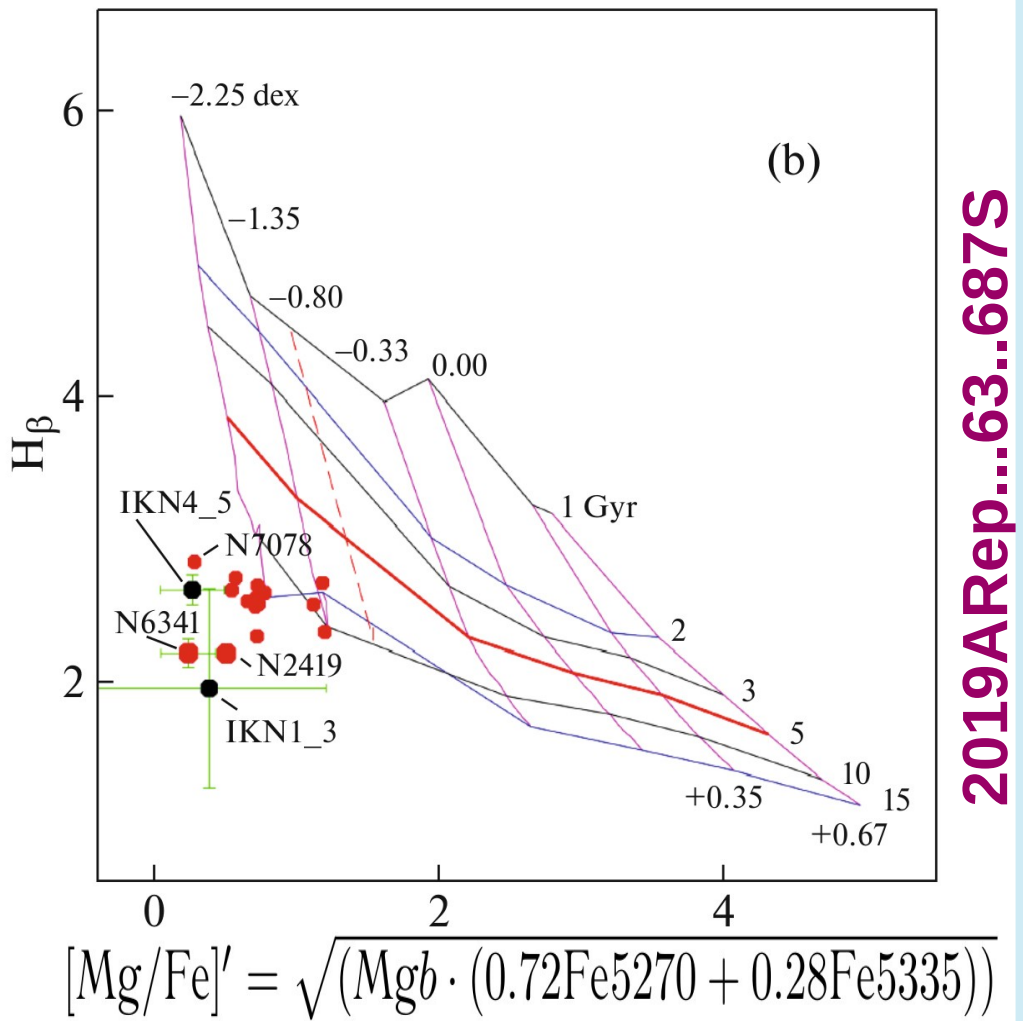
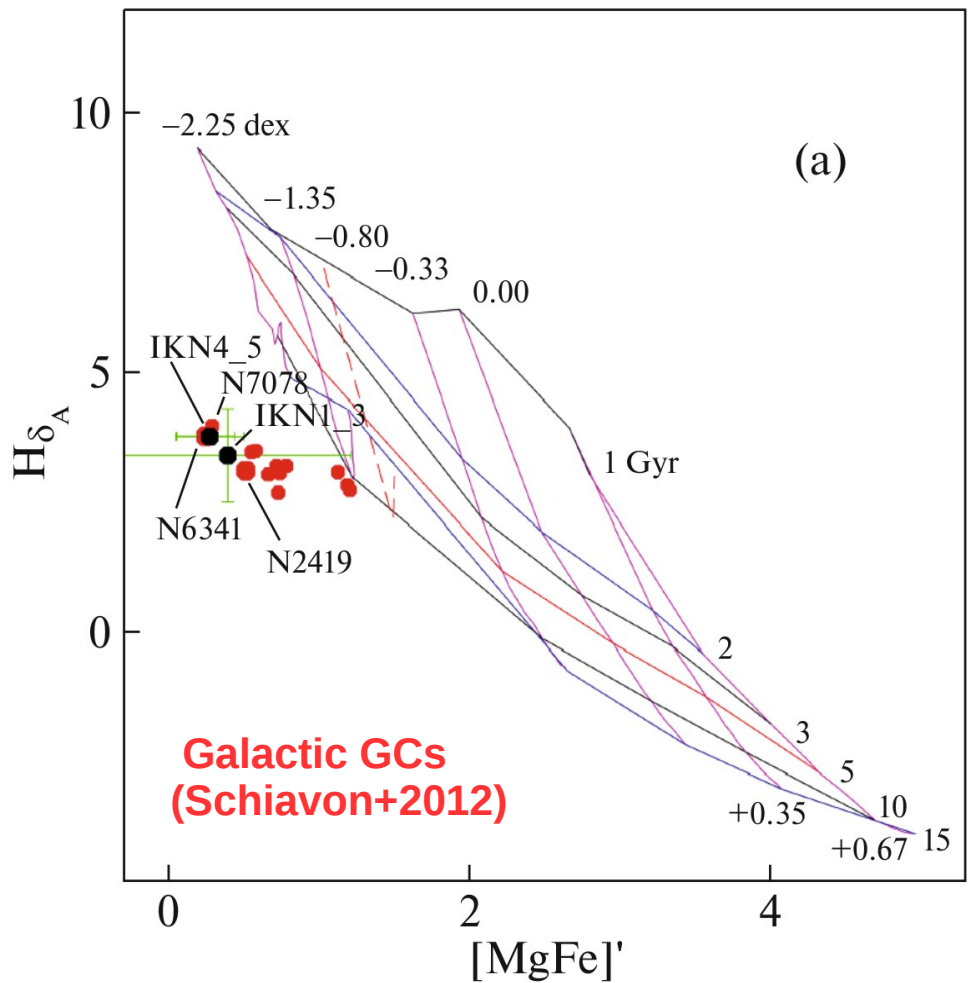
2019ARep...63..687S

IKN1 + IKN3 vs. NGC 3201 ([Fe/H] = -1.6), HBR= (B-R)/(B+V+R)= 0.1)



Comparison of the integrated spectrum of IKN1 + IKN3 with the spectrum of NGC3201 (Schiavon et al., 2005). The results of dividing the spectra of objects by the corresponding model spectra are partially visible, shown by thin solid lines. The lower panels display the results obtained by subtracting the model spectra from the observed cluster spectra. The solid curves in the lower panels show the envelope corresponding to $S/N \sim 18$.

Lick index diagnostic diagrams



2019ARep...63..687S

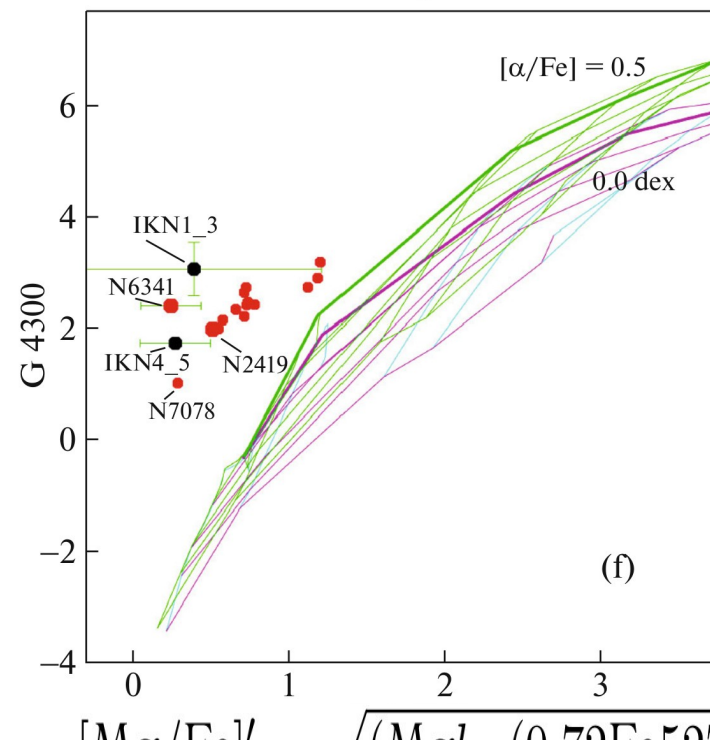
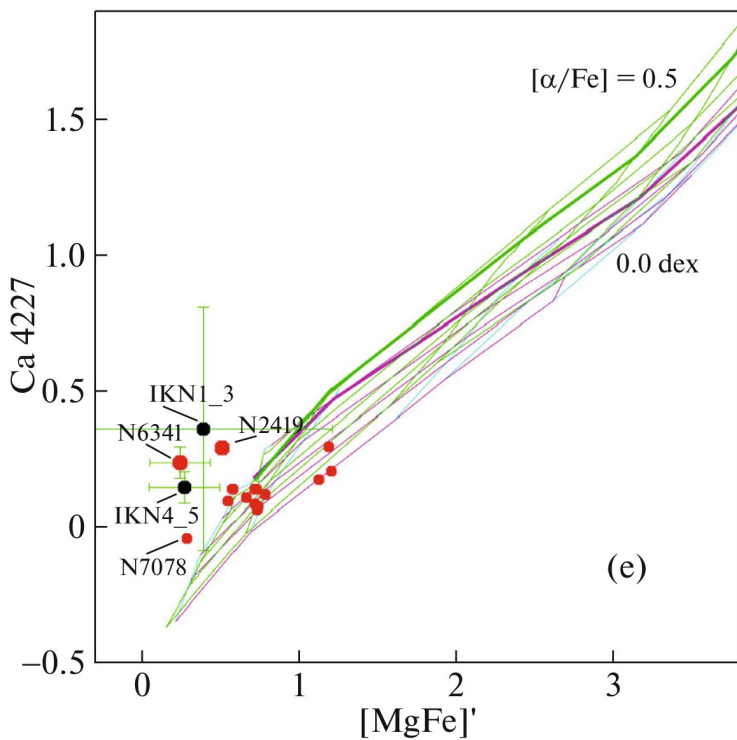
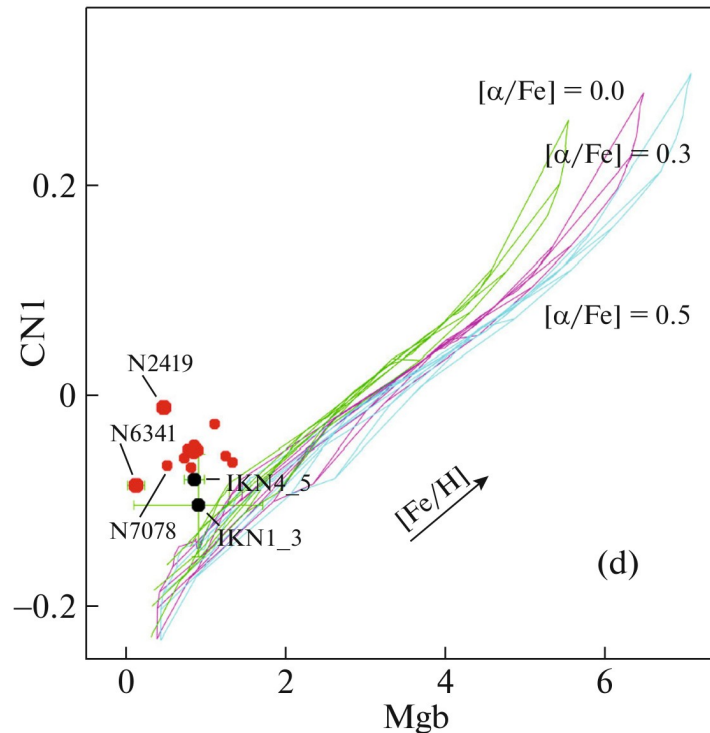
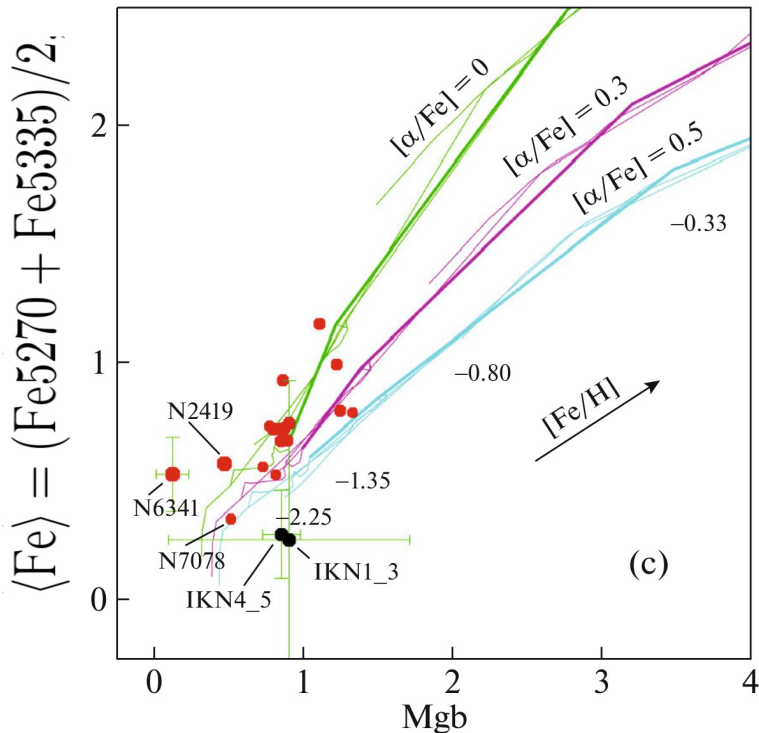
SSP models: Thomas et al. (2003, 2004).

Lick indices are analogs of equivalent widths:

$$I(\lambda) = \left(1 - \frac{\int F_l(\lambda) \Delta\lambda}{\int F_c(\lambda) \Delta\lambda} \right)^{-1} \Delta\lambda,$$

where λ is the wavelength, F_l is the flux in the line, and F_c the flux in the continuum in the vicinity of the line (Burstein et al. 1984; Worthey et al. 1994; Worthey 1994; Worthey & Ottaviani 1997; Trager et al. 1998)

Lick index diagnostic diagrams



$$[Mg/Fe]' = \sqrt{(Mggb \cdot (0.72Fe5270 + 0.28Fe5335))}$$

Results for GCs in IKN dSph (2019ARep...63..687S)

- ◆ Heliocentric radial velocities of the clusters are $V_h = 38 \text{ km/s}$ for **IKN4 + IKN5** and $V_h = -39 \text{ km/s}$ for **IKN1 + IKN3**.
- ◆ Pixel-by-pixel comparison of the spectra with models computed using PEGASE.HR (Le Borgne+2004) and the ELODIE library (Prugniel & Soubiran, 2001) of stellar spectra in the ULYSS program (Koleva+2008, 2009) and lick index diagnostic plots
- ◆ → $[\text{Fe}/\text{H}] = -2.1 \pm 0.2 \text{ dex}$, $T = 12.6 \pm 2 \text{ Gyr}$, $[\alpha/\text{Fe}] \sim 0.5 \text{ dex}$
 $0.3 < [\text{Mg}/\text{Fe}] < 0.5 \text{ dex}$, $[\text{Ca}/\text{Fe}] \sim 0.05 \text{ dex}$,
and $0.1 < [\text{C}/\text{Fe}] < 0.3 \text{ dex}$ for **IKN4 + IKN5**
- ◆ → $-1.6 < [\text{Fe}/\text{H}] < -2.1 \text{ dex}$ and $7 < T < 12.6 \text{ Gyr}$
for IKN1 + IKN3.
- ◆ $H\delta F / H\beta \geq 1.1$ for low-metallicity Galactic globular clusters with blue horizontal branches (Schiavon et al., 2004). Similarity of the majority of the corresponding Lick indices for **IKN4 + IKN5** and **IKN1 + IKN3**, measured from the integrated spectra → similar metallicities and ages.

Population synthesis of integrated-light spectra of star clusters

Sharina M.E., Shimansky V.V., Khamidullina D.A.

Age, Helium Content and Chemical Composition of Globular Clusters in the M31 Neighborhood and in our Galaxy. // Astrophys. Bull. 73 (3) , 337-354. 2018.

Sharina M.E., Shimansky V.V., Kniazev A.Y..

Nuclei of dwarf spheroidal galaxies KKs 3 and ESO 269–66 and their counterparts in our Galaxy. // MNRAS 471, 1955 - 1968. 2017.

Khamidullina D., Sharina M., Shimansky V., Davoust E.

Chemical Abundances in the Globular Clusters NGC 6229 and NGC 6779.// Astrophys. Bull. 69, P. 409-426. 2014.

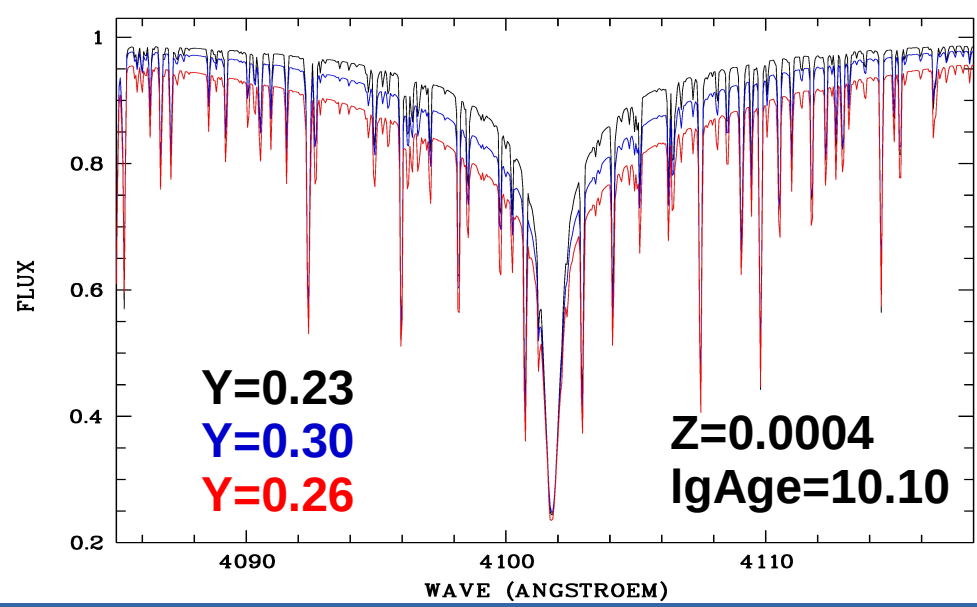
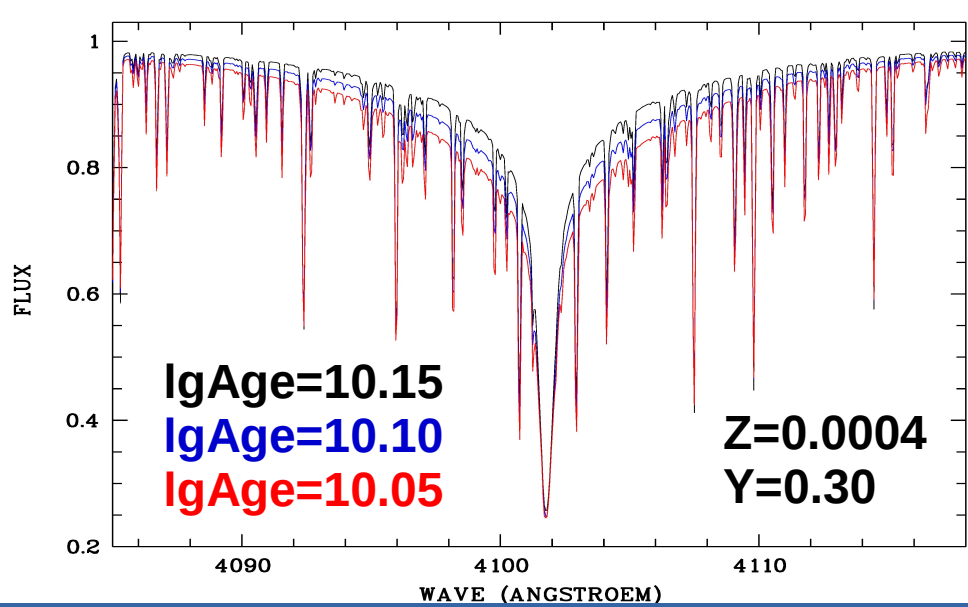
Sharina M.E., Shimansky V.V., Davoust E.

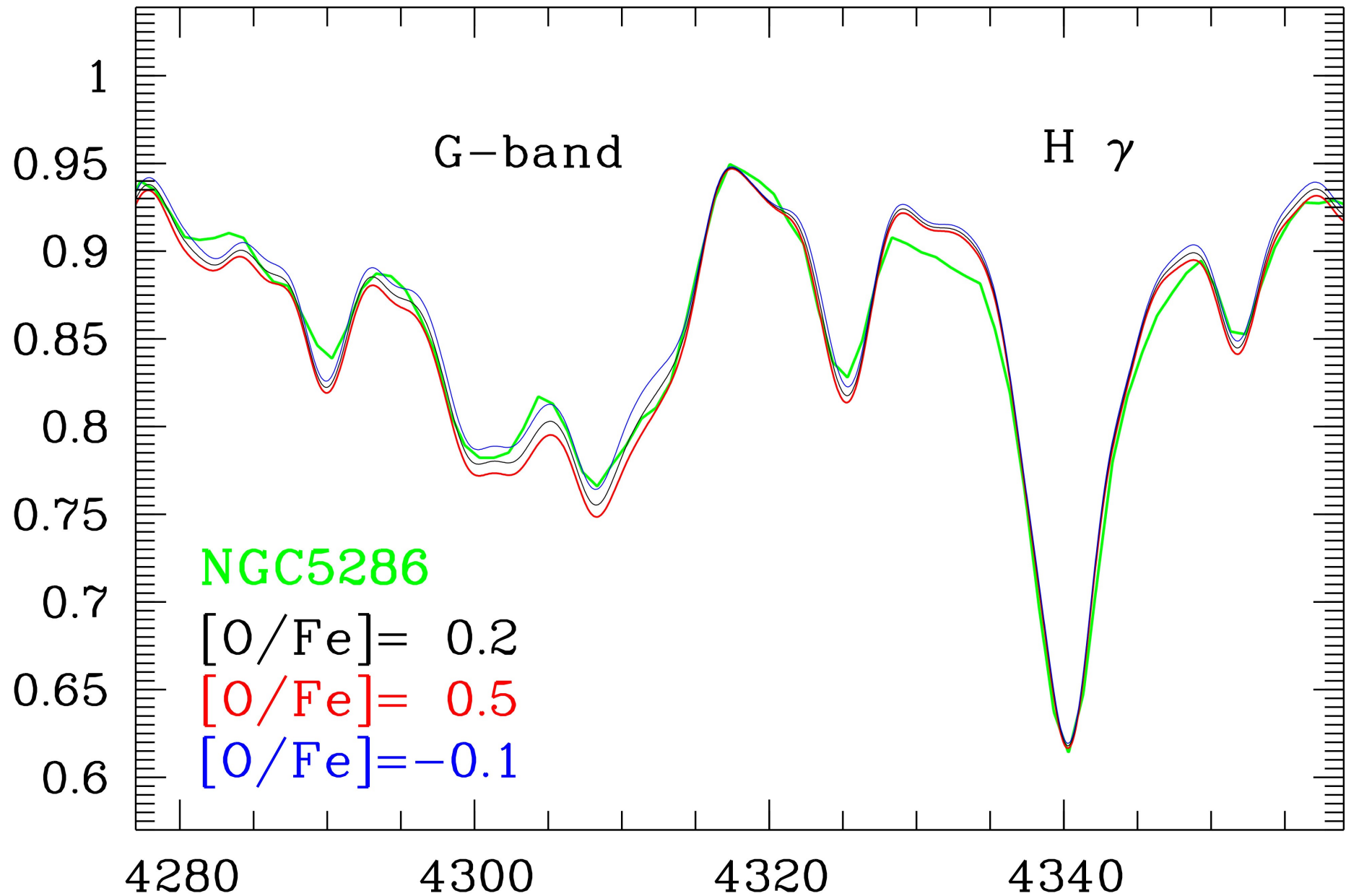
Modeling and Analysis of the Spectrum of the Globular Cluster NGC 2419. // Astron. Reports 57, P. 410-422. 2013.

Population synthesis of integrated-light spectra of star clusters

Sharina M.E. (SAO RAS), Shimansky V.V. (Kazan State Univ.)

- Comparison of **observed spectra** of star clusters and **synthetic integrated-light spectra** → age, Y, [Fe/H], [Mg/Fe], [Ca/Fe], [C/Fe], [Ti/Fe], [Cr/Fe]
- plane-parallel, hydrostatic stellar atmosphere models by Castelli & Kurucz (2003). Synthetic spectra computed using ATLAS9 and SYNTHE codes (Sbordone + 2004).
- Bertelli et al. (2008) isochrones → T eff, log(g), [Fe/H] of stars. Chabrier (2005) MF.
- Broadening of HI lines profiles: Vidal et al. (1973) and Griem (1960)
- Line lists: Kurucz web site (<http://kurucz.harvard.edu/linelists.html>)
- Observational data: medium-resolution spectra (training sample: Schiavon et al. 2005).
S/N ≥ 100, 3900 – 5500Å, resolution FWHM~ 3 – 5 Å



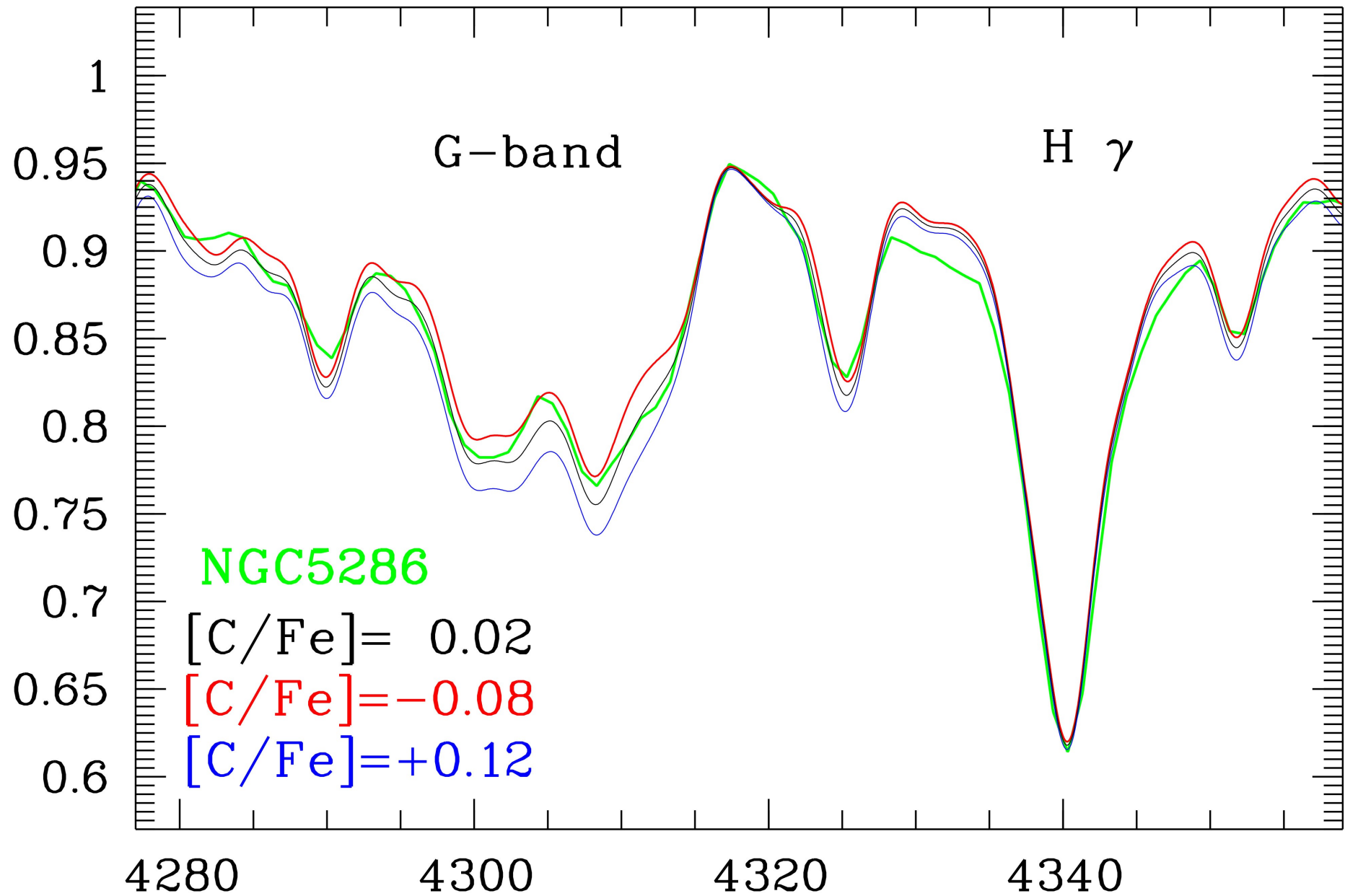


NGC5286

[O/Fe] = 0.2

[O/Fe] = 0.5

[O/Fe] = -0.1



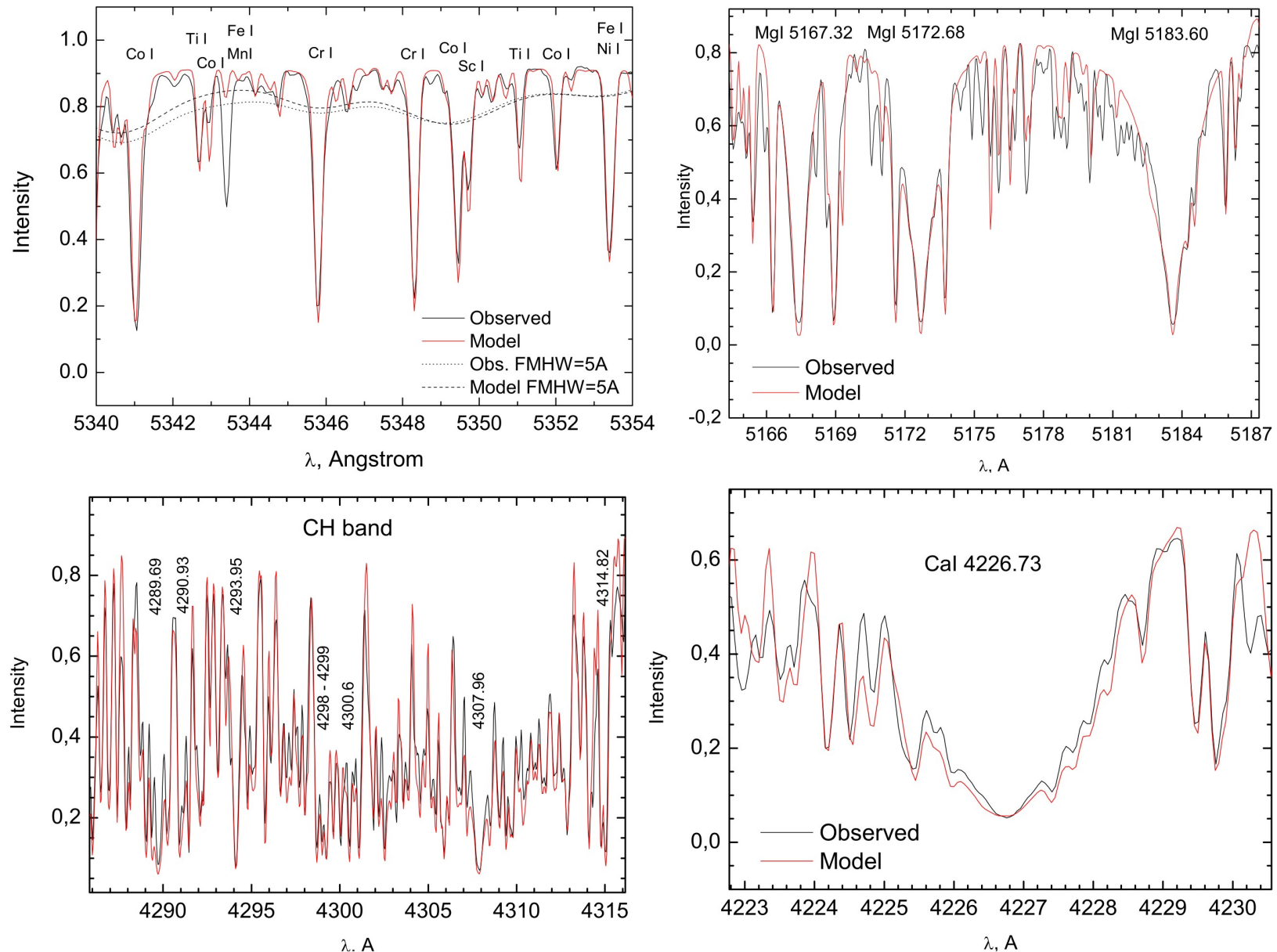
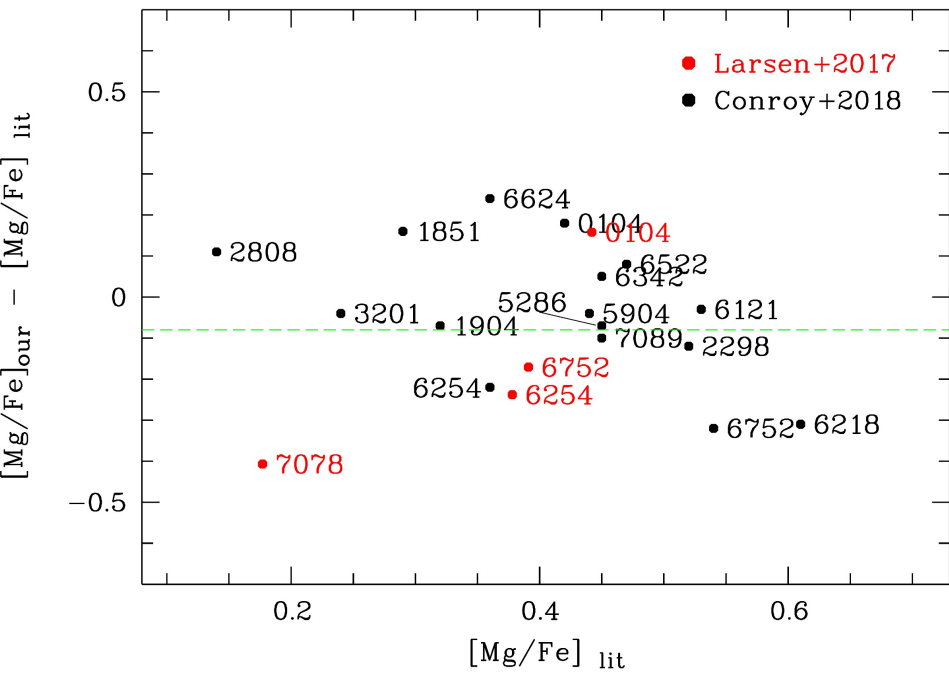
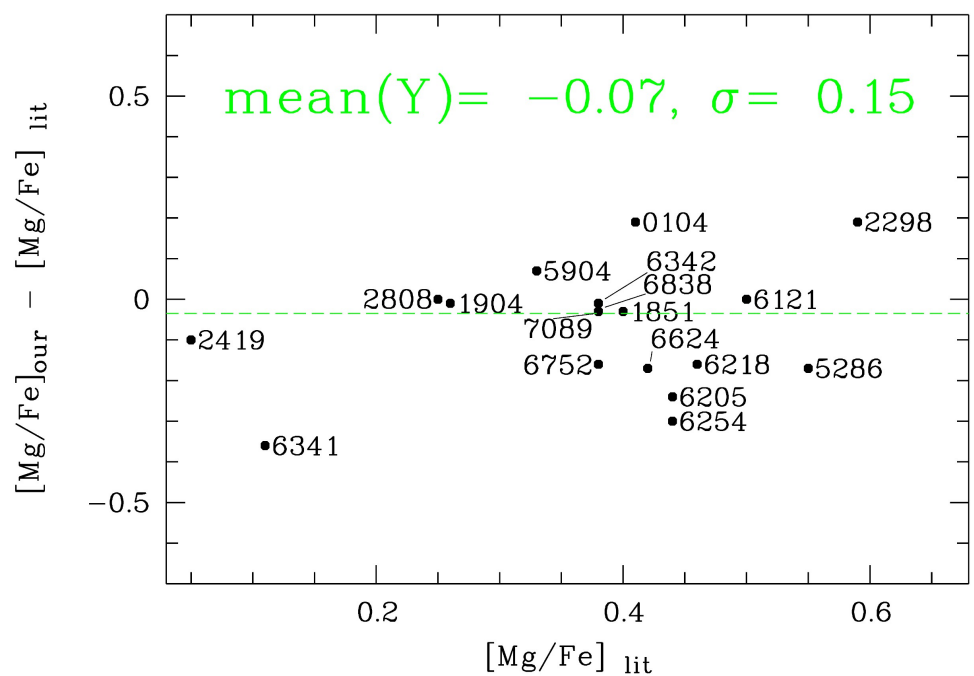
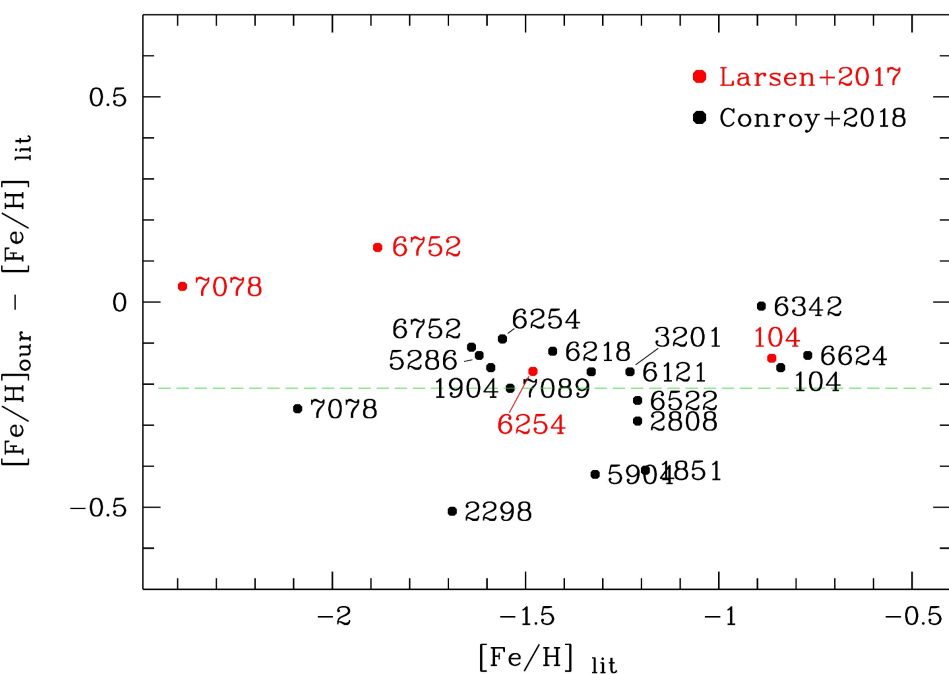
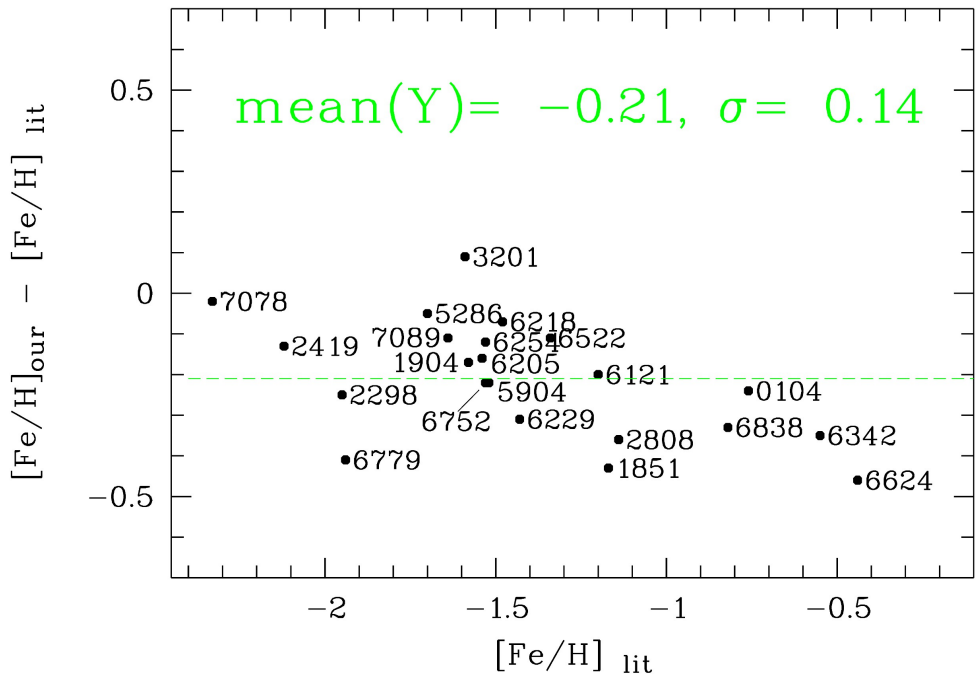
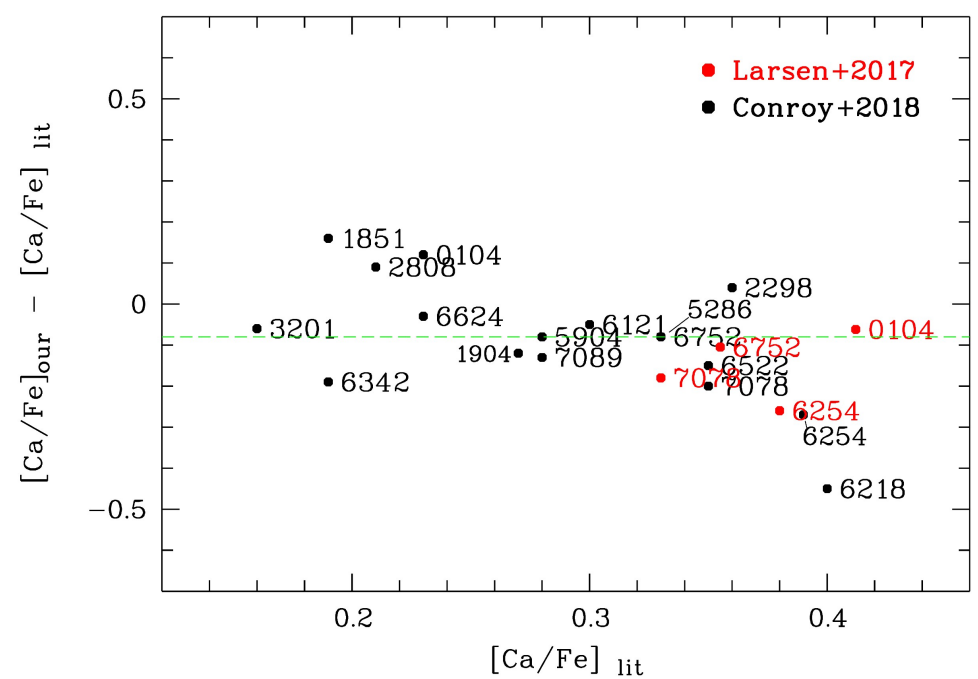
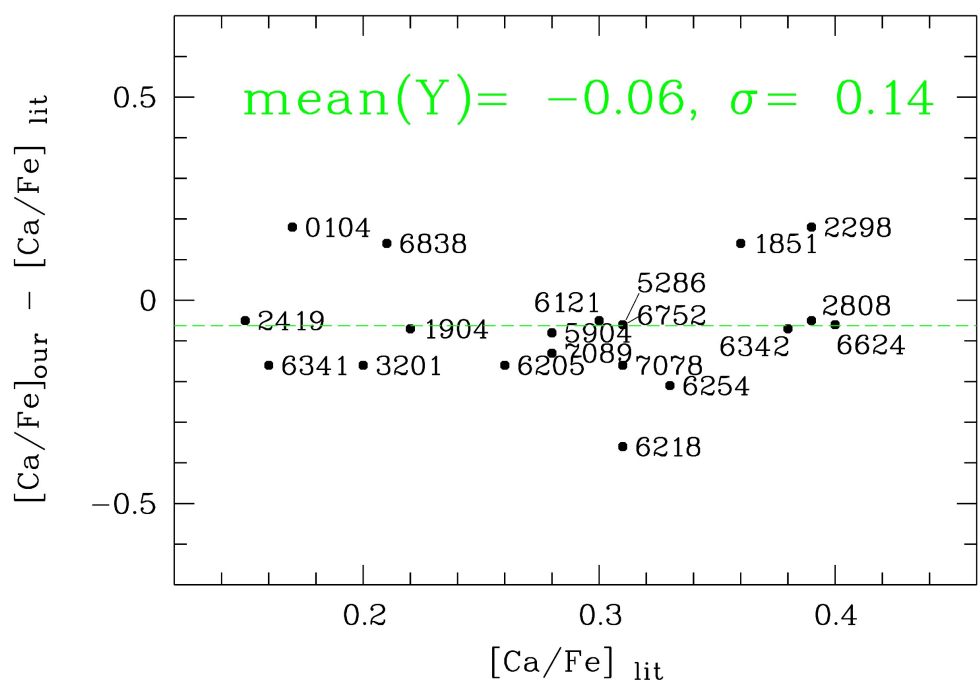
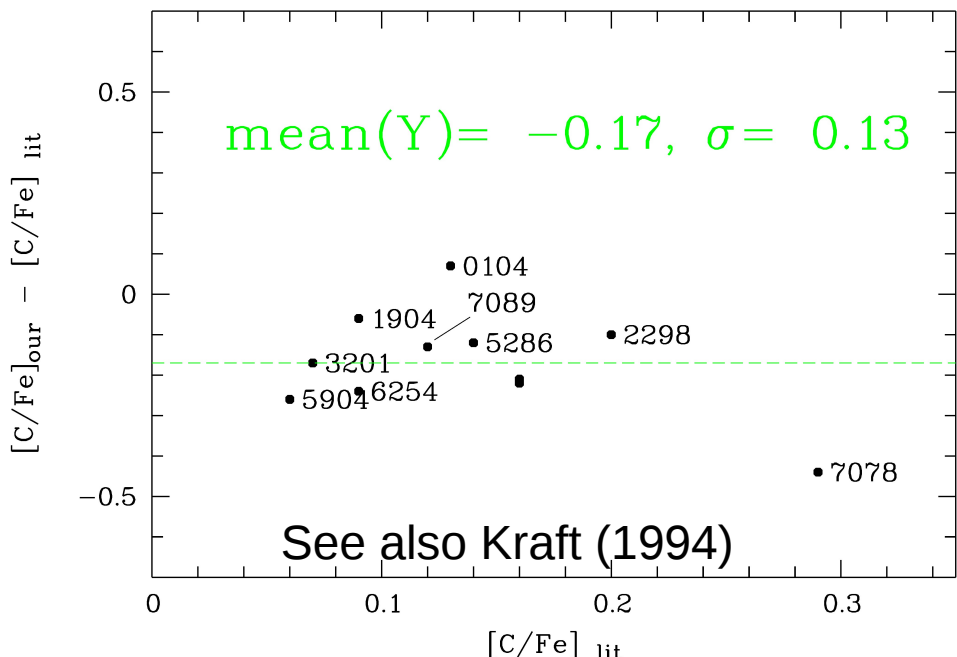
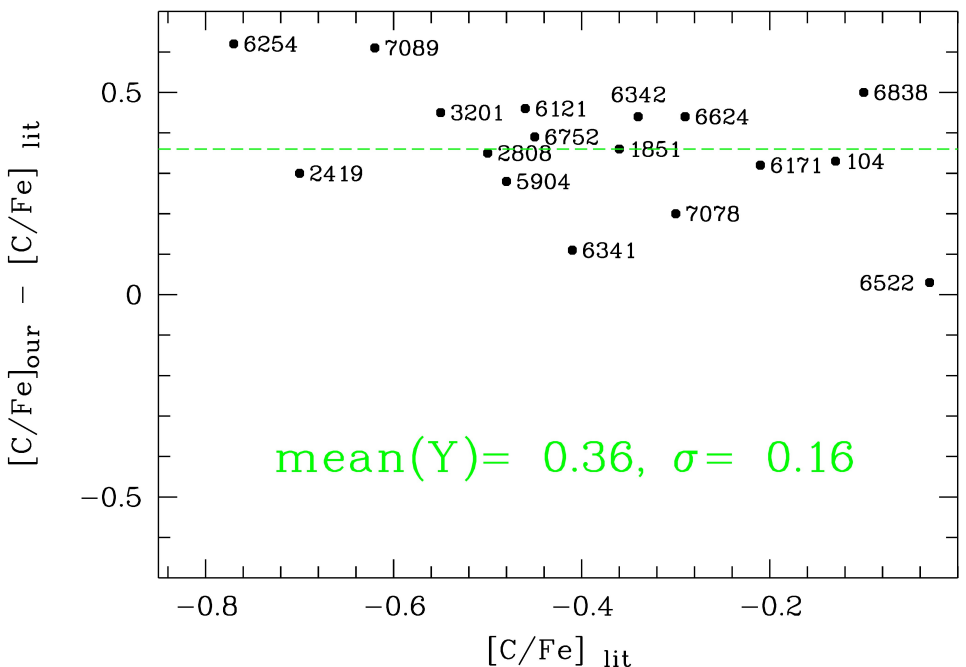


Fig. A.1. Comparison of the observed Arcturus spectrum from the ELODIE database and our calculated synthetic spectrum for a wavelength region including iron peak elements and for three wavelength regions corresponding to several prominent spectroscopic features (CH and MgH molecules, CaII H, K lines, CaI 4227 Å). The adopted parameters are from Ramírez & Prieto (2011).

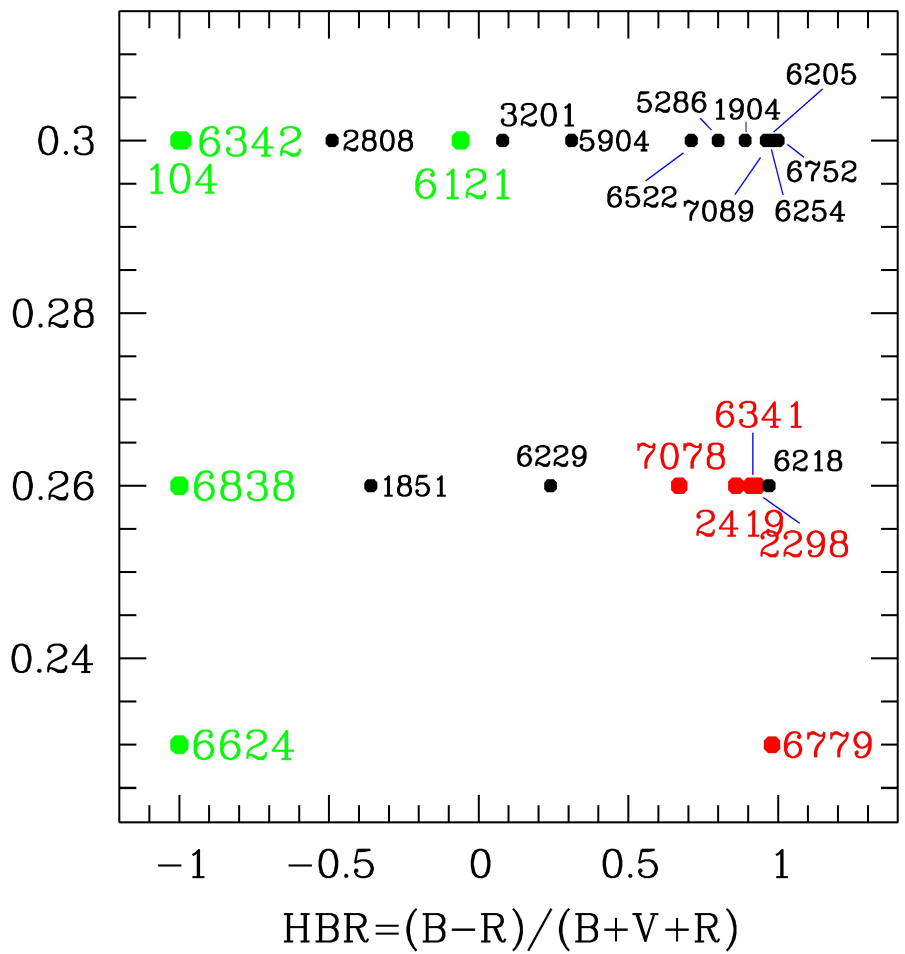
Comparison of the abundances determined using our method with the abundances from high-resolution spectroscopic studies of red giants in the clusters (left) (Pritzl +2005, Roediger + 2014) and with the abundances determined using IL spectra of GCs (right) (Larsen+2017, Conroy +2018).



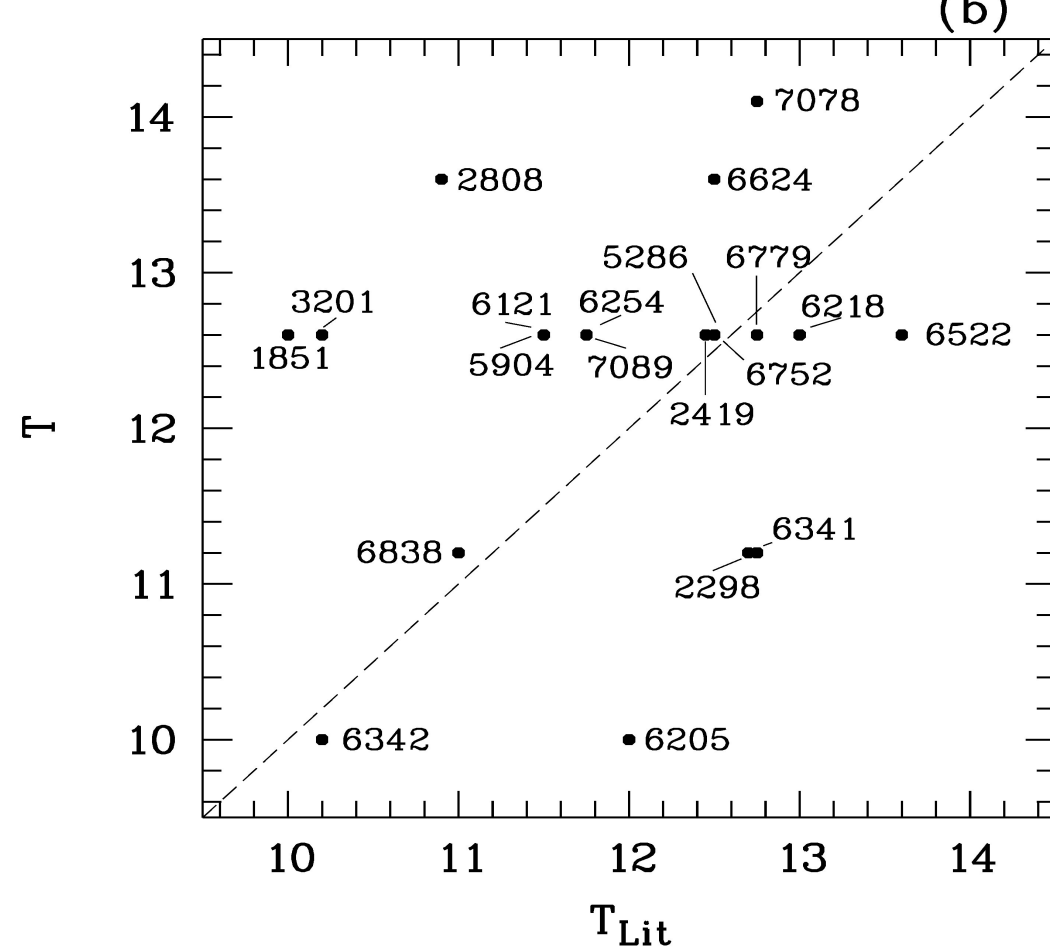
Comparison of the abundances determined using our method with the abundances from high-resolution spectroscopic studies of red giants in the clusters (left) (Pritzl +2005, Roediger + 2014) and with the abundances determined using IL spectra of GCs (right) (Larsen+2017, Conroy +2018).

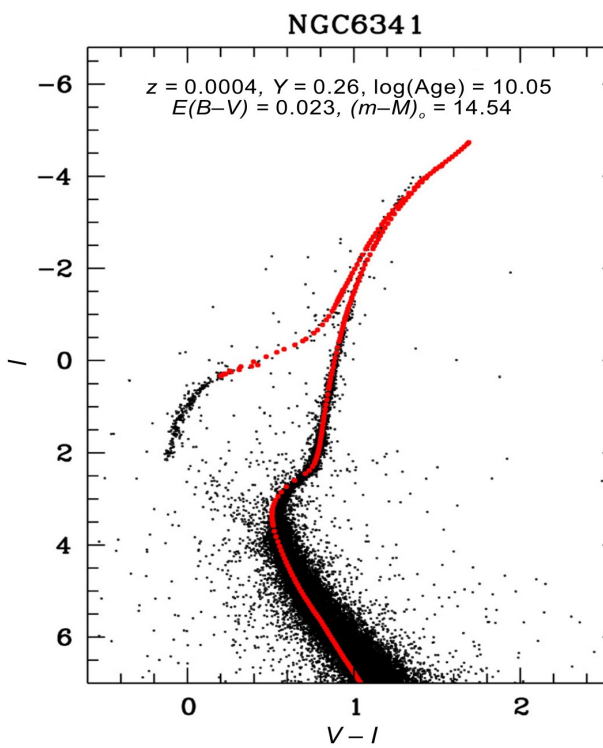
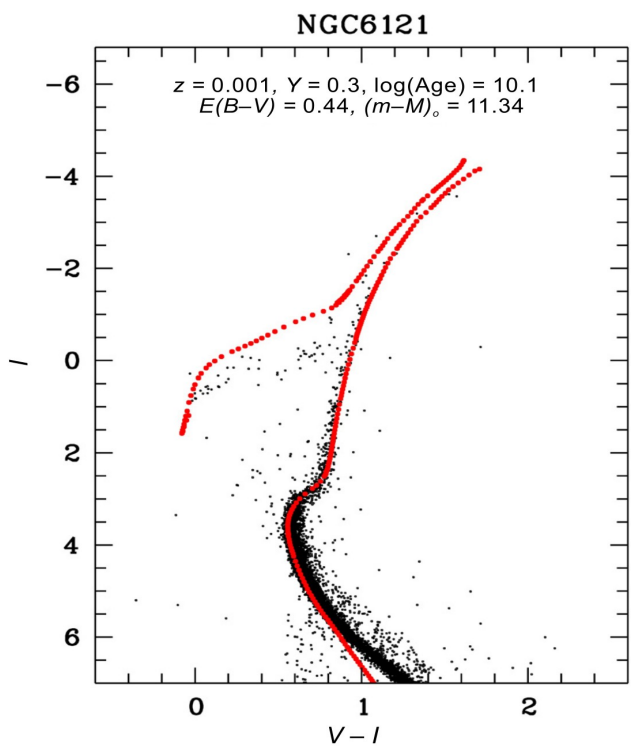
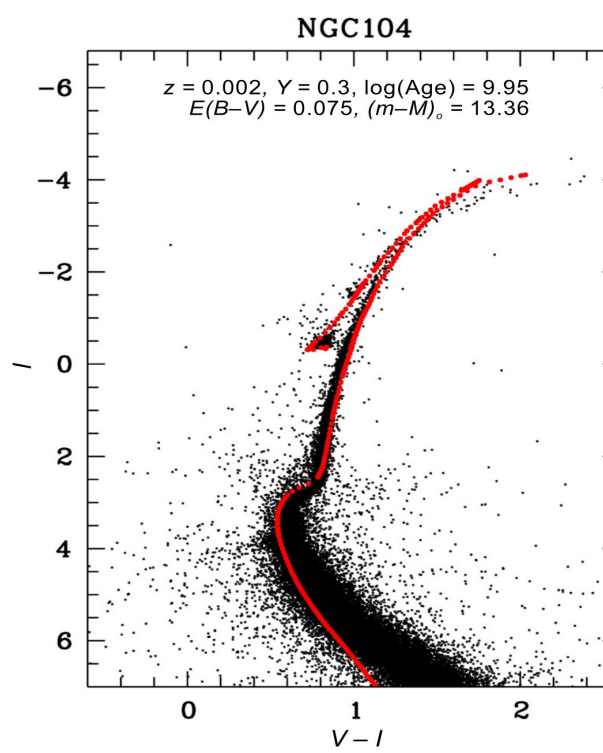
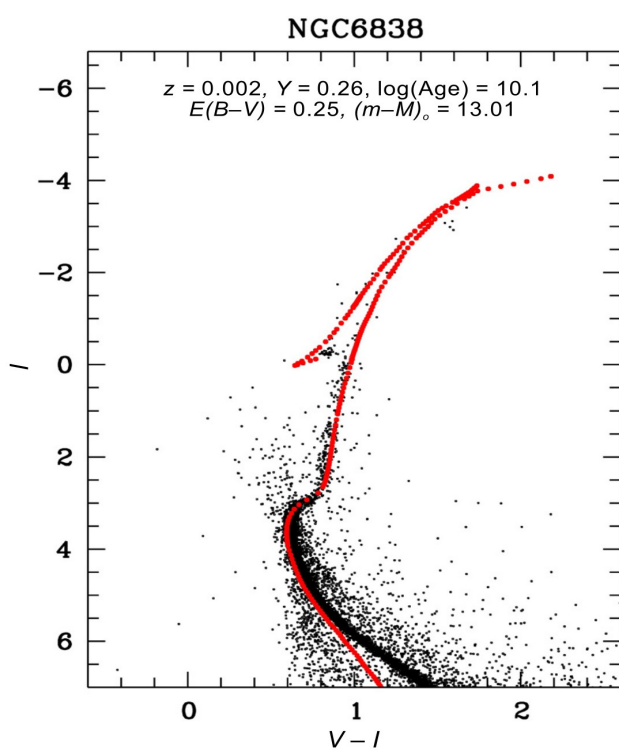


[Fe/H]~−2; [Fe/H]~−1.6; [Fe/H]~−1. (a)



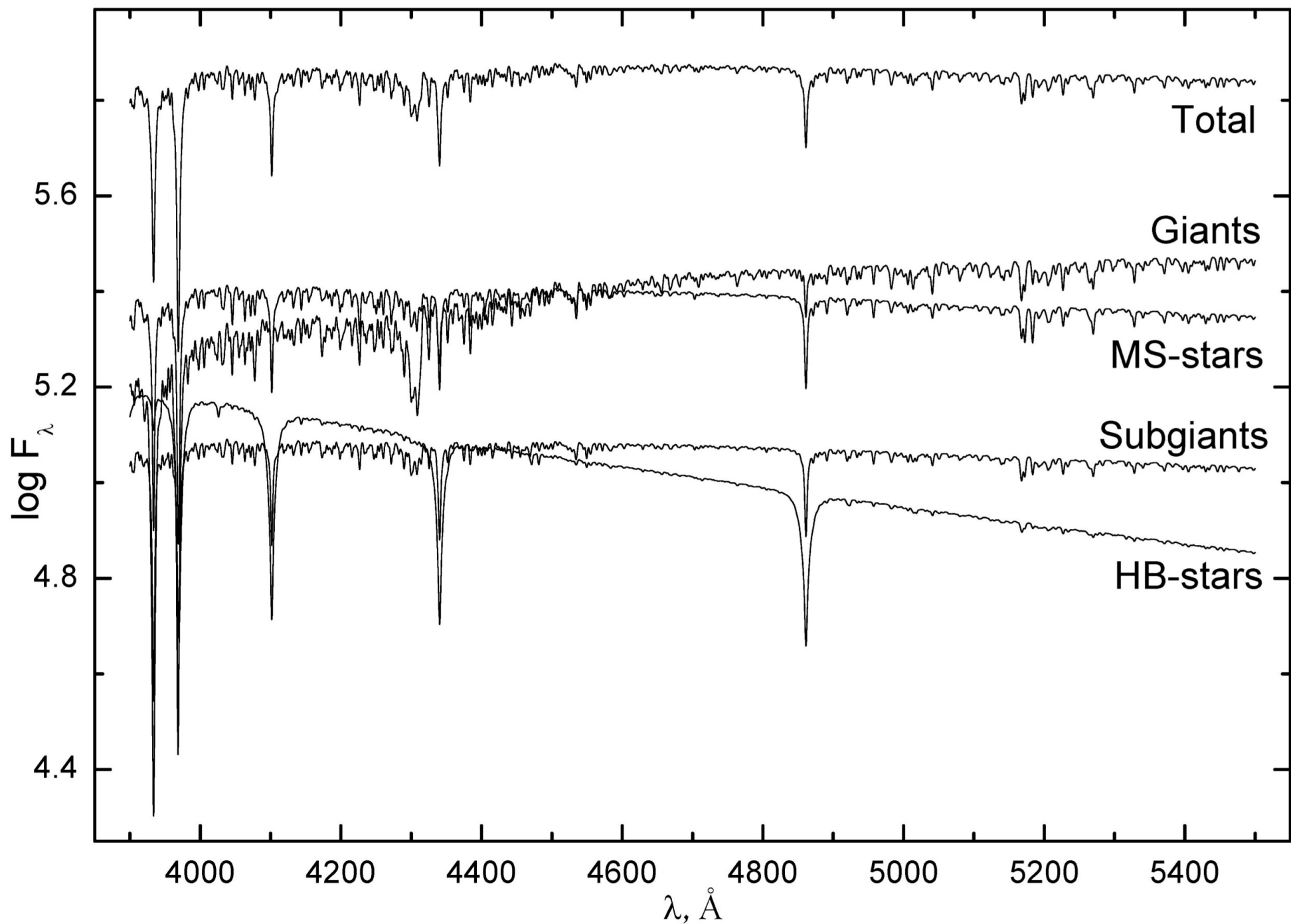
(b)





Sharina M.E., Shimansky V.V., Khamidullina D.A., 2018AstBu..73..318S
 Age, Helium Content and Chemical Composition of Globular Clusters in the M31 Neighborhood and in our Galaxy.

Contribution of different types of stars to the integrated spectrum of N6229



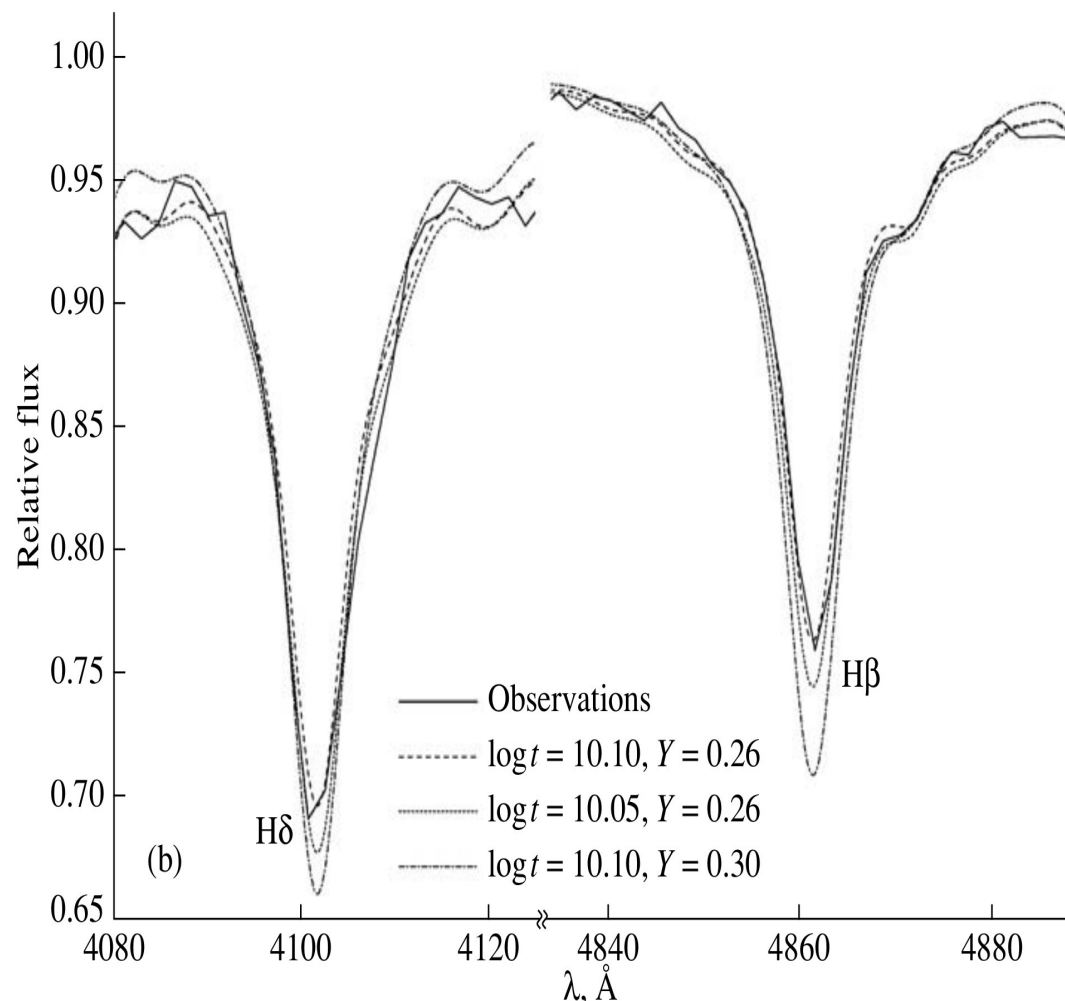
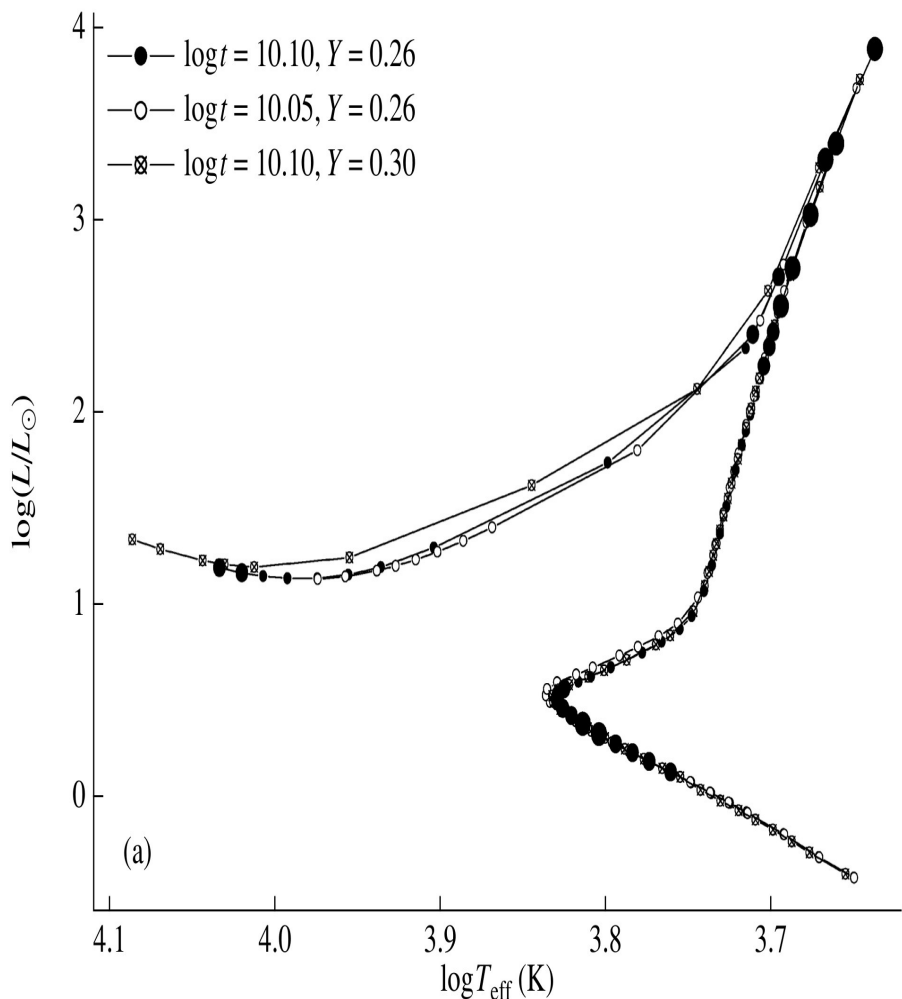
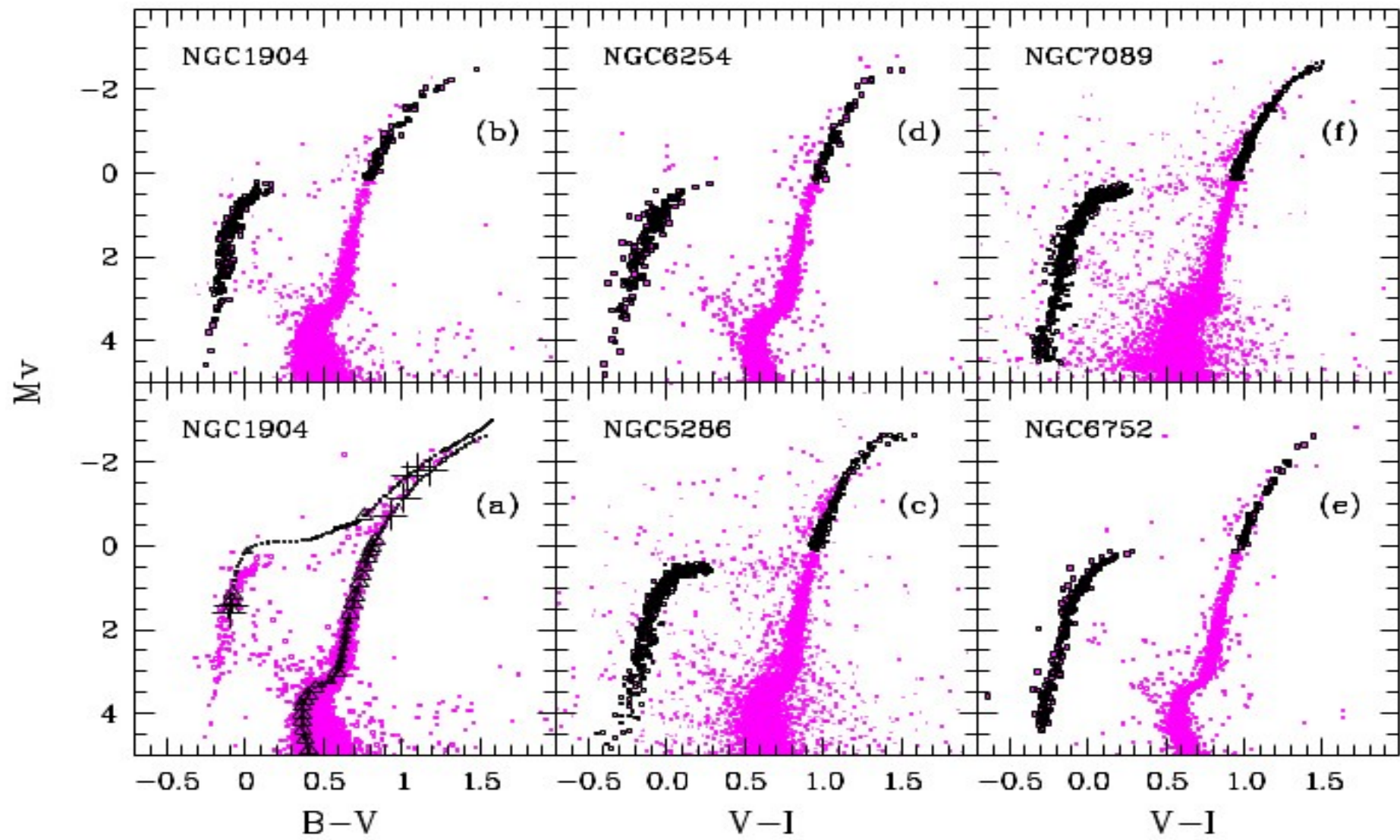


Fig. 2. (a) Isochrones from [22] on $\log T_{\text{eff}} - \log g$ diagrams and (b) H β and H δ line profiles in the integrated spectra of NGC 2419 for several values of the cluster parameters t and Y , assuming $Z = 0.0001$. The various size circles on the $\log t = 10.10, Y = 0.26$ isochrone denote points whose contributions to the cluster's combined light at $\lambda = 5000 \text{ \AA}$ are less than 1%, from 1% to 3%, and more than 3%.

The contribution of HB stars to integrated spectra of GCS with respect to the contribution of RGB stars. These values are shown for 5 GCS and for synthetic spectra calculated with the program CLUSTER and isochrones by Bertelli + (2008):
 (1) $Z=0.0004$, $\log(\text{age})=10.1$, $Y=0.3$, (2) $Z=0.0004$, $\log(\text{age})=10.05$, $Y=0.3$,
 (3) $Z=0.0004$, $\log(\text{age})=10.1$, $Y=0.26$ и (4) $Z=0.0004$, $\log(\text{age})=10.05$, $Y=0.26$.

	NGC 1904	NGC 5286	NGC 6254	NGC 6752	NGC 7089	1	2	3	4
$I_{\text{HB}}/I_{\text{RGB}}$	0.85	0.79	0.79	0.8	0.78	0.77	0.47	0.65	0.54

Sharina et al., 2017MNRAS.471.1955S



The *Hubble Space Telescope* UV Legacy Survey of Galactic Globular Clusters. XVI. The helium abundance of multiple populations

A. P. Milone¹, A. F. Marino², A. Renzini³, F. D'Antona⁴, J. Anderson⁵,
B. Barbuy⁶, L. R. Bedin³, A. Bellini⁵, T. M. Brown⁵, S. Cassisi⁷, G. Cordon¹,
E. P. Lagioia¹, D. Nardiello^{1,3}, S. Ortolani¹, G. Piotto^{1,3}, A. Sarajedini⁸,
M. Tailo¹, R. P. van der Marel^{5,9}, E. Vesperini¹⁰

ABSTRACT

Recent work, based on data from the *Hubble Space Telescope* (*HST*) UV Legacy Survey of Galactic Globular Clusters (GCs), has revealed that all the analyzed clusters host two groups of first- (1G) and second-generation (2G) stars. In most GCs, both 1G and 2G stars host sub-stellar populations with different chemical composition.

We compare multi-wavelength *HST* photometry with synthetic spectra to determine for the first time the average helium difference between the 2G and 1G stars in a large sample of 57 GCs and the maximum helium variation within each of them. We find that in all clusters 2G stars are consistent with being enhanced in helium with respect to 1G. The maximum helium variation ranges from less than 0.01 to more than 0.10 in helium mass fraction and correlates with both the cluster mass and the color extension of the horizontal branch (HB).

These findings demonstrate that the internal helium variation is one of the main (second) parameters governing the HB morphology.

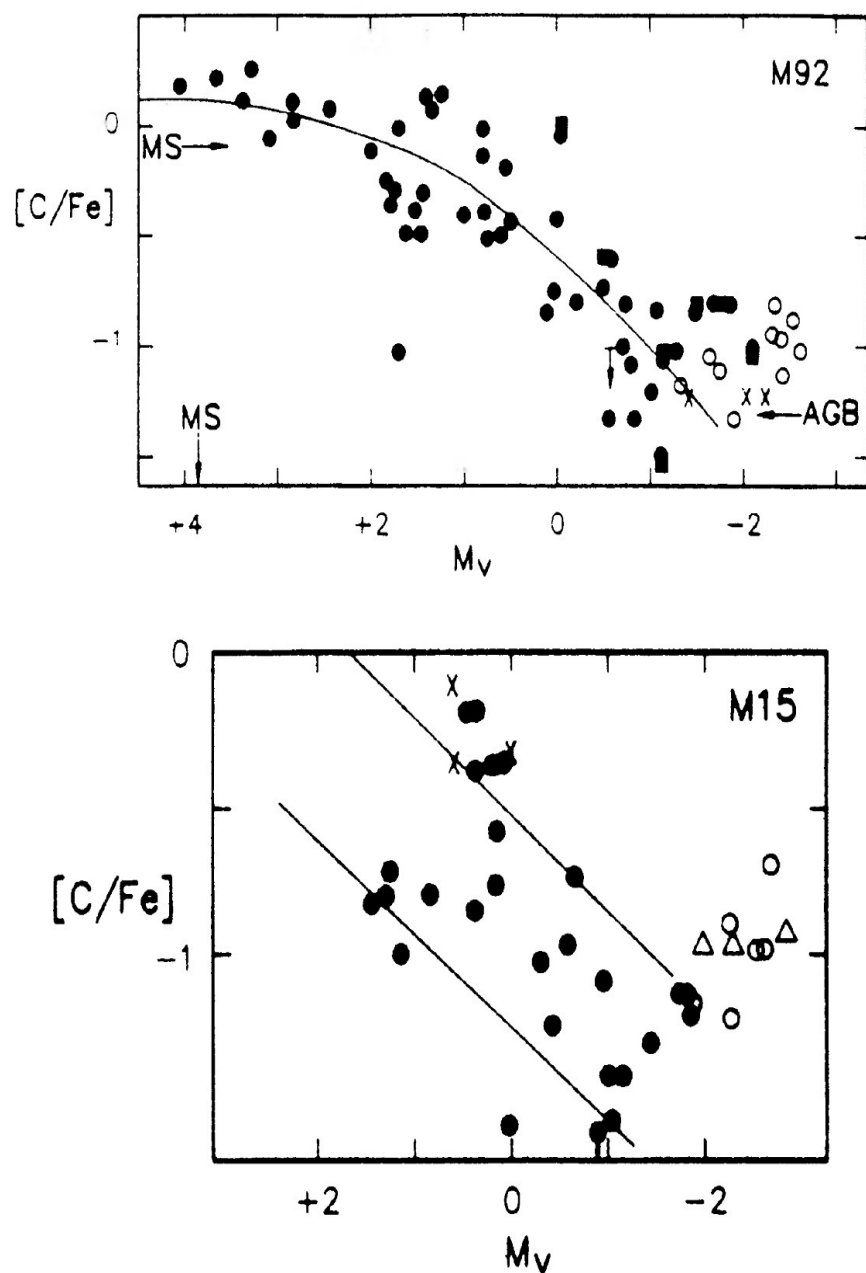


FIG. 5—(After Suntzeff 1989, copyright Obs. de Paris. Reproduced with permission.) Carbon abundances as a function of M_v , i.e., evolutionary state, in M92 and M15. For M92, the closed circles are from Langer et al. (1986), the open circles are derived from studies by Bell (1984) and Stetson

Abundance Differences Among Globular-Cluster Giants: Primordial Versus Evolutionary Scenarios

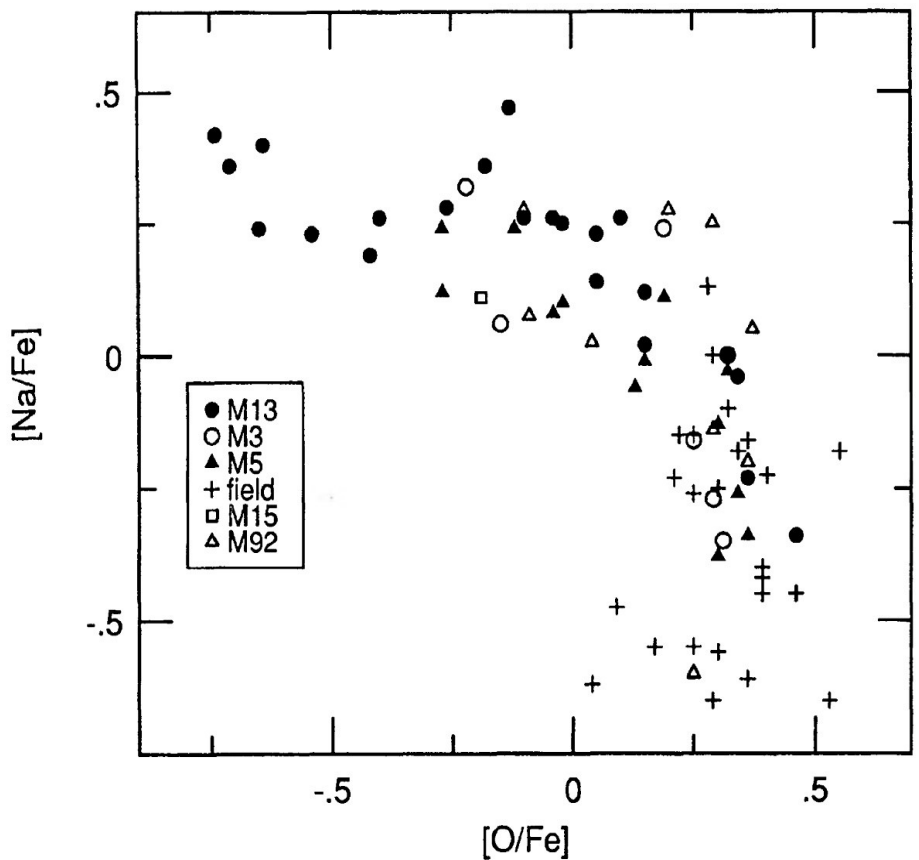
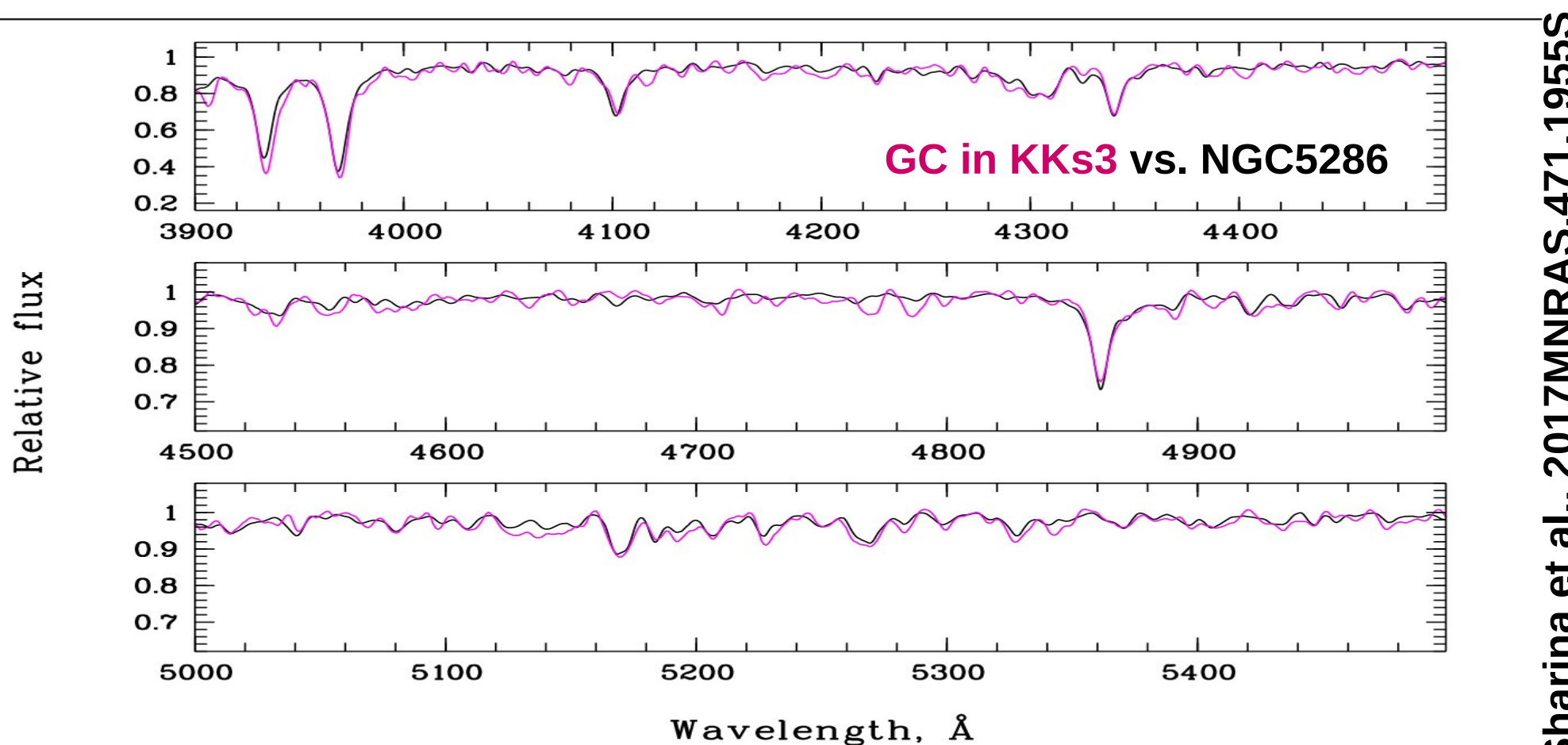


FIG. 8—(After Kraft et al. 1993, copyright American Astronomical Society. Reproduced with permission.) The Na–O anticorrelation among giants in globular clusters and the halo field having metallicities $[Fe/H] < -1$. In the color–magnitude diagram, all cluster stars lie within 1 mag of the red giant tip; the field star sample is dominated by giants having luminosities less than that of the typical cluster giant.

Table 4. Elemental abundances and their uncertainties for the GCs in KKs 3 and E269–66 and for five Galactic GCs according to our measurements using medium-resolution integrated-light spectra (Section 3).

GC	[Fe/H] (dex)	[C/Fe] (dex)	[N/Fe] (dex)	[Mg/Fe] (dex)	[Ca/Fe] (dex)	[Ti/Fe] (dex)	[Cr/Fe] (dex)
In E269–66	-1.50 ± 0.2	-0.12 ± 0.2	0.25 ± 0.4	0.10 ± 0.2	0.00 ± 0.2	0.15 ± 0.3	0.15 ± 0.3
In KKs 3	-1.55 ± 0.2	-0.18 ± 0.2	0.45 ± 0.4	0.15 ± 0.2	0.30 ± 0.2	0.25 ± 0.3	0.05 ± 0.3
NGC 1904	-1.75 ± 0.2	0.03 ± 0.1	0.30 ± 0.3	0.25 ± 0.1	0.15 ± 0.1	0.15 ± 0.2	0.25 ± 0.2
NGC 5286	-1.75 ± 0.2	0.02 ± 0.1	0.35 ± 0.3	0.38 ± 0.1	0.25 ± 0.1	0.15 ± 0.2	0.25 ± 0.2
NGC 6254	-1.65 ± 0.2	-0.15 ± 0.1	0.25 ± 0.3	0.14 ± 0.1	0.12 ± 0.1	0.45 ± 0.2	-0.09 ± 0.2
NGC 6752	-1.75 ± 0.2	-0.06 ± 0.1	0.30 ± 0.3	0.22 ± 0.1	0.25 ± 0.1	0.20 ± 0.2	0.20 ± 0.2
NGC 7089	-1.75 ± 0.2	-0.01 ± 0.1	0.30 ± 0.3	0.35 ± 0.1	0.15 ± 0.1	0.20 ± 0.2	0.20 ± 0.2



Age, Helium Content and Chemical Composition of Globular Clusters in M31

Logarithmic age in years, helium mass fraction and metallicity in dex for GCs in M33 (CBF 98 and CBF 28), for nuclear GCs in dSphs ESO269-66 and KKs3, and for GCs in the M31 neighbourhood ([SD09] GC7, MayallIII, MGC 1 and Bol 298). Results derived using the described method are highlighted in bold.

Object	$\log(T)$	Y	[Fe/H]
CBF 98	10.05 ± 0.05 ⁰	0.30 ⁰	-1.40 ± 0.15 ⁰
	10.04 ± 0.05 ¹	—	-1.30 ± 0.10 ¹
CBF 28	10.0 ± 0.05 ⁰	0.23 ⁰	-1.55 ± 0.15 ⁰
KKs3 GC1	10.1 ± 0.1 ²	0.30 ± 0.03 ²	-1.5 ± 0.2 ²
ESO269-66 GC1	10.1 ± 0.1 ²	0.30 ± 0.03 ²	-1.5 ± 0.2 ²
SD09 GC7	10.0 ± 0.1 ³	0.30 ± 0.03 ³	-1.8 ± 0.1 ³
MayallIII	9.9 ± 0.12 ⁴	—	-1.5 ± 0.2 ⁴ , -1.8 ± 0.3 ⁵
	10.15 ± 0.05 ³	0.26 ± 0.02 ³	-1.00 ± 0.05 ³
MGC 1	10.18 ⁶ , 10.08 ⁷	—	-0.95 ± 0.09 ⁶ , -1.08 ± 0.09 ⁸
	10.0 ± 0.05 ³	0.30 ± 0.03 ³	-2.20 ± 0.1 ³
Bol 298	9.7 ± 0.1 ⁹	—	-2.14 ¹⁰
	10.0 ± 0.1 ³	0.30 ± 0.03 ³	-1.85 ± 0.1 ³
	10.3 ± 0.1 ⁹ , 10.13 ¹¹	—	-2.14 ¹⁰ , -2.07 ± 0.18 ¹¹

Notes: ⁰this work; ¹Sharina et al. 2010; ²Sharina et al. 2017; ³Sharina et al. 2018; ⁴Sharina & Davoust 2009; ⁵Veljanoski et al. 2013; ⁶Meylan et al. 2001; ⁷Ma 2009; ⁸Huchra et al. 1991; ⁹Ma 2012; ¹⁰Mackey et al. 2007; ¹¹Fan et al. 2011.

Conclusions

- Our method of population synthesis of IL spectra of GCs works for old GCs
- We can use it to analyze spectra of GCs, the shape of stellar mass function, the mean He content of GCs.

Thanks for your attention!